Review Article

Nano Research
2024, 17(5): 3472–3492

ISSN 1998-0124 CN 11-5974/O4
https://doi.org/10.1007/s12274-023-6251-4

Recent advances in metal-organic frameworks for electrochemical performance of batteries

Haoyang Xu[1], Pengbiao Geng[2], Wanchang Feng[1], Meng Du[1], Dae Joon Kang[3], and Huan Pang[1] (✉)

[1] *School of Chemistry and Chemical Engineering, Yangzhou University, Yangzhou 225002, China*
[2] *School of Materials Science and Engineering, Suzhou University of Science and Technology, Suzhou 215009, China*
[3] *Department of Physics, Sungkyunkwan University, 2066, Seobu-ro, Jangan-gu, Suwon, Gyeonggi-do 16419, Republic of Korea*

Received: 5 September 2023 / **Revised:** 6 October 2023 / **Accepted:** 8 October 2023

ABSTRACT

Energy shortage hinders the rapid development of today's society, and the emergence of electronic travel equipment alleviates this phenomenon to a certain extent. The batteries are the energy storage part of electric equipment. Metal-organic frameworks (MOFs) are a fresh sort of porous crystal materials with controllable structure, large specific surface area, and adjustable pore size. MOFs are good electrode materials, which are used to make a variety of friendly environment, long cycling life and superior energy density of new batteries. Furthermore, MOFs are also used in separators and electrolytes, which have a lot of application space in batteries. In this review, the up-to-date research advance of MOF materials in various kinds of batteries (lithium-ion batteries, lithium oxygen batteries, lithium sulfur batteries, zinc-ion batteries, potassium-ion batteries, etc.) is reviewed. Moreover, concisely introduced several conventional synthesis approaches of MOFs. Finally, Perspectives and directions on the future improvement of MOF in energy storage devices are proposed for meeting the requirement of practical applications.

KEYWORDS

metal-organic frameworks, synthesis, batteries, cycling performance

1 Instruction

Fossil energy sources accelerate the progress of industry, facilitates people's daily life, and is the basis for promoting the rapid development of human society [1]. In the process of rapid development, people accelerate the use of coal, oil and so on. This behavior accelerates environmental pollution, energy depletion, and limits the development of social industry. However, with the swift advance of today's society and the speedy increase of population, this phenomenon forces people to look for renewable energy and energy conversion technology [2, 3]. In recent years, wind energy source, hydropower, solar energy source, and other renewable resource have been continuously developed, but they are unpredictable, because they are greatly affected by the weather environment [4]. In order to meet the needs of life and production, it is essential to employ high-class energy storage equipment to put these renewable sources into full play [5].

In the current sustainable development of electrochemical energy storage devices, the rechargeable batteries using advanced energy storage technology are the most competitive, and are widely used in a variety of electronic devices [6–8]. At present, lithium-ion batteries (LIBs) have many advantages, such as cycling performance stability and light weight [9, 10]. It has a very wide range of commercial applications in portable electronic devices, electric vehicles, and other emerging applications [11]. Due to the generation of concentration gradient and batteries polarization, the precipitation is uneven, which leads to the formation of lithium dendrite, resulting in poor battery performance and even safety accidents [12–14]. With the purpose of change this situation, researchers have made great efforts in metal oxides and alloys. However, the effect is not ideal, the theoretical capacity is low and the performance is unstable. Thus, it is imperative to expand a novel sort of anode materials for LIBs to satisfy today's energy demand [15, 16]. In recent years, many different kinds of metal-organic frameworks (MOFs) have been utilized as electrode materials for inversible LIBs. After continuous exploration by scientists, it has been found that this is due to their structural diversity and large specific surface area. The peculiar fabric of MOF enhances the conversion rate during the reaction process by offering numerous lithium storage locations and increasing the contact area between electrodes and electrolytes, further improving battery performance [17–19].

MOFs also gone by the name of porous coordination polymer or porous coordination network, are a type of organic–inorganic hybrid materials formed by organic ligands and metal ions [20, 21]. Its unique crystal porous structure, highly dispersed metal composition, and adjustable pore size can not only obtain outstanding electrochemical stability from its solid structure, but also ensure high capacity through rich electroactive centers materials [22, 23]. In addition, they are widely used in various fields of society, including catalysis, fluorescence, adsorption, drug delivery and catalytic energy storage, and bring various conveniences to people's life [24–26]. In recent years, as a new type of electrode material, unique functionality MOFs have been paid more and more attention by researchers, and have come to be a pop theme in the territory of chemistry and materials science, and have progressed swiftly in the domain of electric energy storage in today's world development trend [27–30].

Address correspondence to huanpangchem@hotmail.com, panghuan@yzu.edu.cn

In recent years, although there have been many reports on the simple synthesis methods of MOFs and their application studies in different fields. However, there is no intuitively clear summary of the performance effects of the direct application of pristine MOFs in the field of batteries. Therefore, in order to have a visual and detailed understanding of the latest research on MOF materials in the field of batteries in Scheme 1, to compare their performance characteristics, and to promote new developments in the field of batteries, we have conducted a brief review of the latest research on MOFs materials in the field of batteries. This review summarises the simple synthesis methods, morphological features and electrochemical performance data of MOFs in various types of batteries, comprising LIBs, lithium sulfur batteries (LSBs), lithium oxygen batteries (LOBs), potassium-ion batteries (KIBs), zinc-ion batteries (ZIBs), etc. Finally, some challenges and development directions of MOFs in batteries are put forward.

2 Synthesis of MOFs

The coordination of organic ligands with metal ions has long been the cornerstone of synthetic chemistry, which is used to build materials on a wide range of length scales [31–35]. MOFs are come into being by the alignment of metal ions or organic junctions around metal ion agglomerates, so it is also called porous coordination network or porous coordination polymer [36, 37]. These porous structures have been highly concerned by professional scientific researchers in the direction of sensor design,supercapacitor, absorption, molecular sieves, gas storage,and electrocatalysts [38, 39]. In conventional synthesis of MOFs, a certain amount of solvent is first added to the autoclave (typically more than two-thirds of the autoclave capacity is added to ensure high pressure in the reactor). Next, the reactants providing metal ions and ligands are added to the autoclave and stirred for a certain time to be well dispersed in the solvent. Finally, it is heated above the boiling point of the solvent at a certain temperature and kept for a period of time to form the desired structure of MOFs [40–42].

After systematic research, specialized researchers found that the type of metal, organic linker and targeting agent determine the synthesis method of MOFs to some extent. There are many factors that affect the functionality and morphology of the final synthesized MOF materials. Even if the synthesis is performed starting from the same reaction starting materials, the synthesis method and conditions can affect the morphology, crystal structure and porosity, resulting in MOFs with different structures and properties. In addition to the commonly used hydrothermal synthesis, there are many other well-established methods, such as ultrasonics, microwave heating, electrochemical methods, and mechanochemical synthesis [43, 44]. Various synthesis methods have their own advantages and have prepared MOFs materials with novel structures and excellent properties, which have broadened the development and applications of MOFs to a certain extent.

Compared with traditional methods, the electrosynthesis possesses has the advantages of low synthesis time, low temperature requirement, diverse structural changes of MOFs, and easy collection of synthesized MOFs [45, 46].

2.1 Solvothermal synthesis

Most MOFs are organometallic compounds synthesized by mixing metal ion nodes or clusters with ligands containing different functional groups under solvothermal conditions [47, 48]. High boiling point solvents such as acetonitrile, acetone, ethanol, methanol, dimethylformamide (DMF), and diethyl formamide were generally used in the experiment [49]. The reaction is generally carried out in an autoclave (closed container) under the control of temperature and pressure. In conventional solvothermal synthesis, small-scale electric heating, and high-flux solvothermal synthesis in small bottles or sealed nuclear magnetic resonance tubes are powerful tools that can not only accelerating the exploration of new MOFs architectures and optimize the synthesis protocol [50]. *In-situ* synthesis of *hericium erinaceus*-like copper-based MOF (HECMs) with graded characteristics of monkey mushroom analogues was carried out by solvothermal method in Fig. 1(a) [51]. However, this method is limited by such factors as long reaction time, high reaction temperature, and high price of reaction solvent. Therefore, the experiments generally use more environmentally friendly and cheaper hydrothermal methods to cover up the solvent cost [52].

2.2 Microwave-assisted synthesis

Microwave heating starts from the inside of the system and heats it from the inside out. The high-frequency magnetic field heats the molecular structure rapidly, and the temperature of the reaction system reaches the required temperature quickly, speeding up the chemical reaction process [53]. Microwave-assisted synthesis is a rapid method for the synthesis of MOFs, which has been widely used in the rapid synthesis of nano-porous materials under hydrothermal conditions. The rapid synthesis of Zr-based MOF (Zr-fum-fcu-MOF) was carried out by dissolving $ZrOCl_2{\cdot}8H_2O$ and fum in DMF assisted by microwave with irradiation power of 800 W in Fig. 1(b) [54]. Microwave-assisted synthesis is predicated on electromagnetic radiation and dipole moment mutual effect of

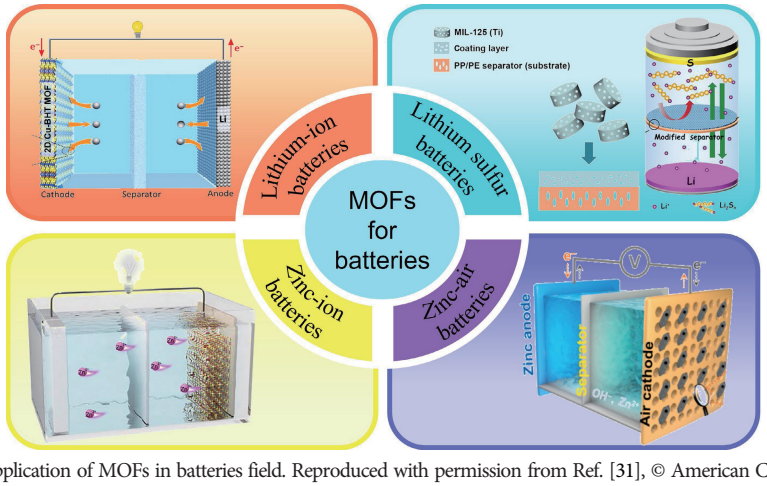

Scheme 1 Illustration of direct application of MOFs in batteries field. Reproduced with permission from Ref. [31], © American Chemical Society 2020. Reproduced with permission from Ref. [32], © Ye, Z. Q. et al. 2021. Reproduced with permission from Ref. [33], © American Chemical Society 2020. Reproduced with permission from Ref. [34], © Elsevier B.V. 2022.

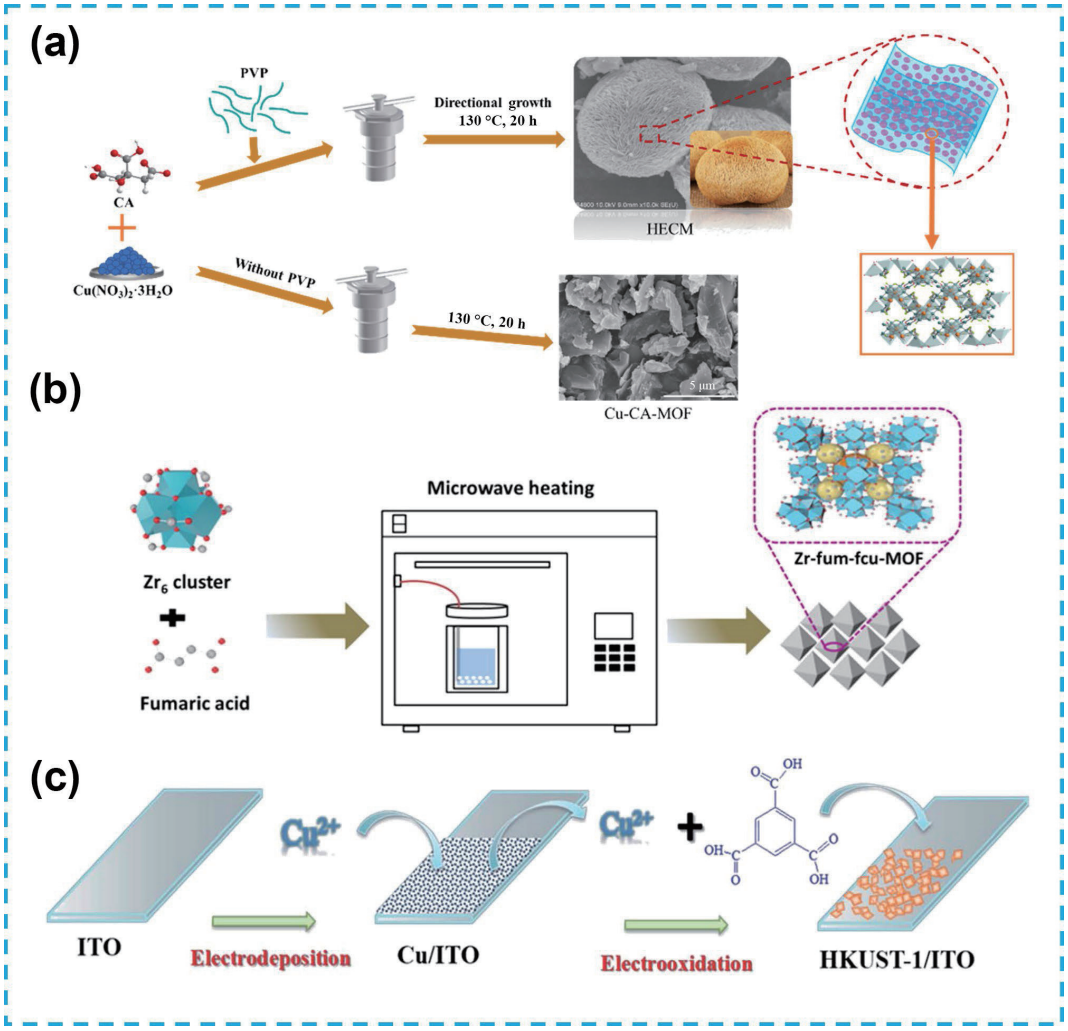

Figure 1 (a) Flow chart for the preparation of MOF-5 by solvothermal synthesis. (b) The schematic diagram of preparation of Zr-fum-fcu-MOF via microwave-assisted heating method. (c) Schematic diagram of HKUST-1 membrane prepared rapidly by electrochemical synthesis method. (a) Reproduced with permission from Ref. [51], © American Chemical Society 2021. (b) Reproduced with permission from Ref. [54], © Elsevier B.V. 2021. (c) Reproduced with permission from Ref. [58], © Jiang, L. L. et al. 2017.

molecules, such as polar solvent molecules or ions in solution [55]. Chromium containing MOFs (Cr-MIL-100) was the first MOFs to adopt this approach. This synthesis technology has many advantages. In addition to rapid crystallization, the potential advantages of microwave-assisted synthesis include uniform heating of the reaction temperature regime, narrow particle size distribution and easy morphology control, and the preparation of MOFs materials with high phase purity [56, 57]. However, this technique is affected by irradiation time, temperature, and solvent concentration.

2.3 Electrochemical synthesis

HKUST-1 ($Cu_3(BTC)_2$; BTC^{3-}: 1,3,5-benzenetricarboxylate) is the first Cu-MOF homogeneous film synthesized on Cu substrate by anodic synthesis method in Fig. 1(c) [58]. Anodic synthesis is a commonly used method in electrochemical synthesis to prepare MOFs. Under the conditions of electrolysis, the anode metal loses electrons to be converted into metal ions, which later combine with ligands on the electrode surface to form MOF [59]. The anodic synthesis method enables the rapid synthesis of MOFs in a short period of time, reduces the demand for solvents and saves resources. Moreover, the synthesized MOFs have high porosity and the morphology of continuously synthesized particles can be controlled, but the method has low yield and is prone to by-products [60, 61]. Compared with the traditional synthesis method, the electrochemical synthesis of MOFs has the advantages of lower temperature, disassociation of negatively charged ion such as NO^{3-}, Cl^- and the compound solution does not need solvent cycle to achieve high Faraday efficiency [62, 63]. However, solvents, electrolytes, electric voltage, current flow density, and temperature have certain effects on the productive rate and structural characteristic of the synthesis method [64].

2.4 Other synthetic

In addition to the above synthetic methods, sonochemical synthesis and mechanochemical synthesis are also mature synthetic methods that have been used in experiments. Sonochemical synthesis is a synthetic method that uses ultrasonic radiation to create and rupture gas bubbles in the solvent to create a high-temperature and high-pressure environment, resulting in more homogeneous nucleation, shorter crystallization time and smaller microcrystalline size [65, 66]. Mechanochemical synthesis is a synthetic method to form MOFs by breaking the bonding structure of the material by mechanical force and van der Waals force reaggregation. This method not only saves resources and reduces the pollution to the environment, but also is a high-quality choice for the synthesis of large quantities of MOFs [67, 68]. In addition, MOFs can be synthesized by electrostatic spinning, spray drying and liquid phase diffusion. Different synthesis methods have their own advantages and disadvantages, and the selection of appropriate synthesis methods is conducive to the experiments and also promotes the further development of MOFs materials.

3 Application of MOFs in batteries

3.1 MOFs for LIBs

To alleviate energy scarcity and find energy alternatives, society has turned its attention to renewable energy storage systems [69]. The high energy density LIBs were born as a traditional energy storage technology and is widely used in portable electronic devices, which greatly facilitates people's daily life and links resource problems [70, 71]. LIBs consist of the following components: a cathode electrode made of lithium transition metal oxide (typically lithium manganate or lithium cobaltate) [72], a specially molded polymer film (the film has a microporous structure that allows lithium ions to pass freely but not electrons) [73], an organic electrolyte, an anode electrode made of activated carbon, and a metal casing. Graphite can be used as an anode material for LIBs. It is regarded as the most popular anode material due to its low cost, abundant and easily available raw materials, enhanced electrical conductivity, high temperature resistance with good thermal conductivity, good mechanical processability, and stable performance [74]. However, graphite-based LIBs undergo a slow decline in capacity. This is the result of poor charging/discharging stability of graphite electrodes and is also related to the multiple use of the battery with temperature [75–77]. Metal oxides can provide more charge storage space and have high energy density, good chemical stability and corrosion resistance. They provide good electrode materials for the development of LIBs and are of great interest to researchers. Nevertheless, its poor electrical conductivity, high production cost, and serious volume changes during long cycles [31, 78]. Therefore, the development of more cost-effective electrode materials for LIBs has been the goal that researchers need to overcome [79].

MOFs are a class of porous crystalline materials with a multidimensional network structure formed by combining a central metal core and an organic ligand [80, 81]. Their structure is controllable and diverse, tailorable, simple to synthesize and easy to manipulate. Due to their outstanding properties in various aspects, MOFs are the most promising and irreplaceable materials in the field of energy storage, especially in the field of batteries [82–84]. Chen et al. synthesized MOFs-177, which was the first application as anode material for LIBs and showed good electrochemical performance [85, 86]. A good foundation for the application of MOFs in LIBs was laid. As a new type of electrode material, MOF shows the following outstanding advantages: (i) abundant raw materials, low cost and green environment; (ii) unique porous structure is conducive to the penetration of electrolyte; (iii) highly symmetrical polymer characteristics can effectively alleviate the problem of organic small molecules easily soluble in electrolyte [87, 88]; and (iv) the rich variety of electroactive sites enables micro-regulation of voltage, capacity and energy density through the design of molecular structures, providing unlimited possibilities for the optimization of battery systems [89, 90]. However, it has been found by scientific research that the MOF-based anode materials have low active site utilization, which limits the battery capacity to some extent. This is caused by the single electro redox active site. In addition, a sharp decrease in electrochemical performance may occur during long electrochemical cycling. This is caused by the continuous decay of the ligand interaction and the collapse phenomenon of the MOF structure. Therefore, the design with multiple oxidation reaction active centers to overcome the low reversible capacity and poor long-cycle stability is an important research direction in the field of battery electrode materials [91].

The channels offered by the column layer framework structure can improve the performance of Li to some extent. It proffers more reactive active sites for the embedding/de-embedding of Li^+ and alleviates the volume expansion at the long cycle [92]. Lei and co-workers prepared a binuclear MOFs of $Co(BDC)TED_{0.5}$ (BDC: 1,4-benzenedicarboxylate and TED: triethylenediamine) with a columnar structure for the anode materials of LIBs in Fig. 2(a) [93–95]. Performance comparison by varying different reaction times in the same environment. The effect of reaction time on performance was summarized, so that the MOF with the best performance could be selected as the anode material in Fig. 2(b). The sheet-like porous framework consisting of loosely stacked thin nanosheets can facilitate rapid ion transport during electrochemical processes, thereby enhancing the electrochemical properties of LIBs in Fig. 2(c) [96]. After comparison $CO(BDC)TED_{0.5}$@24 h exhibits the best electrochemical performance among all materials in Fig. 2(d). This is due to the rapid transfer channels for Li^+ and electrons provided by the interconnected nanosheet stacks.

$Co(BDC)TED_{0.5}$@24 h with convoluted nanosheet stacks exhibited good electrochemical performance as LIBs anode material. The specific capacity of the battery reached 808.2 $mAh·g^{-1}$ even after one thousand performance cycles at 1.0 $A·g^{-1}$ in Fig. 2(e) [97, 98].

Compared with the single-metal organic framework, the bimetallic organic framework can maximize the structural advantages and realize the synergistic impact of multi-ingredients [93]. It has been found by scientific research that the performance of bimetallic organic frameworks in batteries is much better compared to monometallic organic frameworks. Therefore, Li's group members prepared bimetallic organic frameworks by doping 1,2,4,5-benzenetetracarboxylic acid esters of manganese and cobalt to display higher capacity and better multiplicative properties [99]. The flower-like Ni-Co-BTC MOFs synthesized by conventional solvothermal method exhibit high capacity and excellent multiplicative performance in LIBs. The capacity reached 2981 $mAh·g^{-1}$ during the first discharge at a current density of 200 $mA·g^{-1}$ in Fig. 2(f) [100]. During the long cycle, the battery reached 1258 $mAh·g^{-1}$ by the time the current density reached 200 $mA·g^{-1}$ again in Fig. 2(g) [101]. Furthermore, during constant current charge/discharge measurements, Li^+ inserts into (or detaches from) the carboxylic acid group and the benzene ring without directly binding to the metal ion, which is the mechanism of Li storage in Fig. 2(h) [102].

During energy storage and release from LIBs, MOFs with porous structures are prone to slumping, which limits the electrochemical performance. To solve this problem, a special MOFs glass anode was discussed by Li et al. [94]. Cobalt-ZIF-62 (ZIF = zeolitic imidazolate framework) is melt-quenched to form a glass, followed by the addition of carbon black to increase the electrical conductivity, resulting in the desired MOFs glass anode. Cobalt-ZIF-62 is melt-quenched to form a glass, followed by the addition of carbon black to increase the electrical conductivity, resulting in the desired MOFs glass anode in Fig. 2(i) [103]. Because its open network structure has the characteristics of high disorder and high energy state, this new cathode shows extraordinary lithium storage capabilities, such as greater cycling reliability in Fig. 2(j). The lithium-ion storage volume of the MOFs glass anode continues to increase as the charge/discharge cycle progresses, finally reaching twice the previous capacity after 1000 cycles in Fig. 2(k) [104].

Sheet-like bimetallic organic frameworks Ni-Mn-MOFs were synthesized in an autoclave by a modified conventional hydrothermal method. Then, the MOF nanosheets were assembled into three-dimensional (3D) microspheres in Fig. 3(a) [105]. The 3D microspheres of Ni-Mn-MOFs have a unique laminar porous structure that exhibits high specific surface area

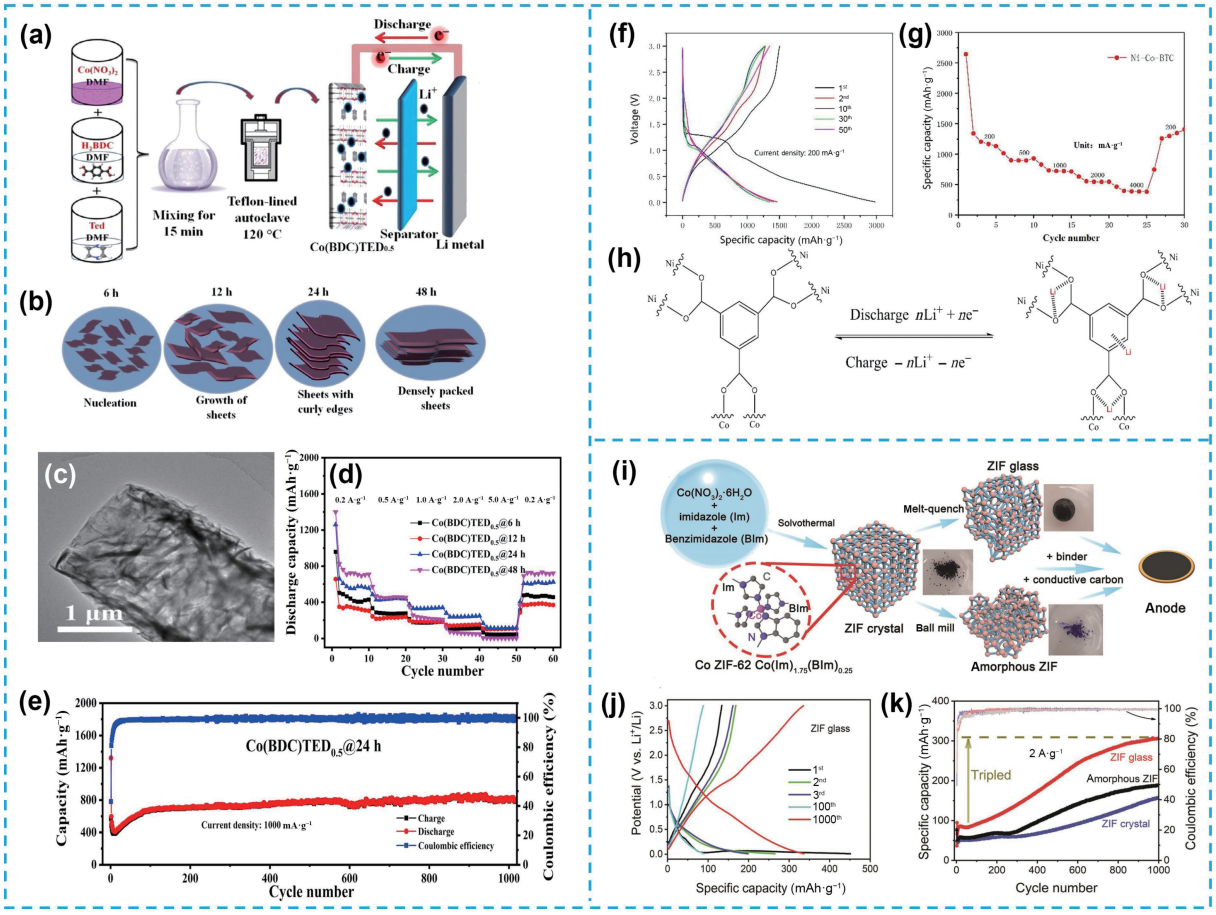

Figure 2 (a) Synthesis process of Co(BDC)TED$_{0.5}$. (b) Co(BDC)TED$_{0.5}$ at different times. (c) Transmission electron microscopy images of Co(BDC)TED$_{0.5}$@24 h. (d) Multiplicity performance at various current densities. (e) Cycling performance at 1000 mA·g^{-1} current density. (f) Constant current charge/discharge curves at 200 mA·g^{-1}. (g) Multiplicity performance at different current densities. (h) The embedding/de-embedding mechanism as anode for LIBs. (i) Synthesis of different morphologies of ZIF by different synthetic methods. (j) Charge–discharge curves of ZIF glass at 1 A·g^{-1}. (k) Cycling performance at 2 A·g^{-1}. ((a)–(e)) Reproduced with permission from Ref. [95], © Elsevier Ltd. 2020. ((f)–(h)) Reproduced with permission from Ref. [99], © The Royal Society of Chemistry 2020. ((i)–(k)) Reproduced with permission from Ref. [103], © Wiley-VCH GmbH 2022.

and potential electrochemical properties. This special structure provides an efficient transport pathway for Li ion transport, thus improving the electrochemical performance of LIBs in Fig. 3(b) [106, 107]. However, during the synthesis process, the hole structure of MOFs was clogged due to the absorption of a large quantity of ethylene glycol. This leads to the electrochemical properties of the assembled LIBs to become poor in Fig. 3(c) [108]. Ni-Mn-BPTC-e-MOFs (BPTC: 3,3',4, 4'-benzophenone-tetracarboxylate) as cathode materials exhibited a high specific capacity of 1380 mAh·g^{-1} at a current density of 100 mA·g^{-1} in Fig. 3(d). After two hundred performance cycles, the battery capacity was slightly lower compared to the previous one when 100 mA·g^{-1} was reached again, and the capacity retention was maintained at about 92% in Figs. 3(e) and 3(f). This finding again shows that overdose of ethylene glycol can have a negative impact on battery performance [109].

LIBs often suffer from HF erosion due to in-built water, which causes the problem of short battery life. However, it has been found in the research community that MOFs can be used not only as electrode materials but also as separator to achieve water removal [106]. Compared with other water removal additives, Cu-BTC MOFs exhibit a different color under various humidity conditions. Reversible water molecules can be reduced by this unique feature (Fig. 3(g)). The quantitative analysis of the thermogravimetric analysis (TGA) curves revealed that the pre-dried MOFs contained 8.1 wt.% water, further confirming the strongly dehydrating capability of Cu-BTC MOFs (Fig. 3(h)) [110]. Using Cu-BTC MOFs with water removal effect as a diaphragm provides stable voltage distribution for LIBs, thus improving the battery life.

Also, its initial voltage polarization is much lower than other LIBs (Fig. 3(i)). LIBs using MOFs with built-in dehydrating agents as diaphragms exhibit good cycling stability even under severe environmental conditions. After up to four hundred performance cycles, the capacity retention rate is still over 72% in Figs. 3(j) and 2(k) [111]. In addition, the MOFs-based built-in water remover exhibits good stability. During long performance cycling, the overall morphological structure did not change significantly even under an electrolyte with strong corrosive properties in Figs. 3(l) and 3(m) [112].

3.2 MOFs for lithium metal batteries (LMBs)

As of now, LMBs are deemed to be the most prospective to replace LIBs with graphite as the cathode material as the new generation of energy storage systems for electric vehicles. This is due to its large capacity of 3860 mAh·g^{-1} and the small electrode potential of the lithium metal cathode [113–115]. Nevertheless, lithium precipitation occurs with the chemical reactions and physical processes within the battery. The occurrence of lithium dendritic problems seriously affects the lifetime and electrochemical performance of the battery, further limiting its development in the market [116, 117]. The controllable and diverse morphologies of MOFs have attracted much attention from the research community in the field of electrochemical energy storage. In addition, MOFs can be used as electrolyte and diaphragm in batteries and can be effective in suppressing Li

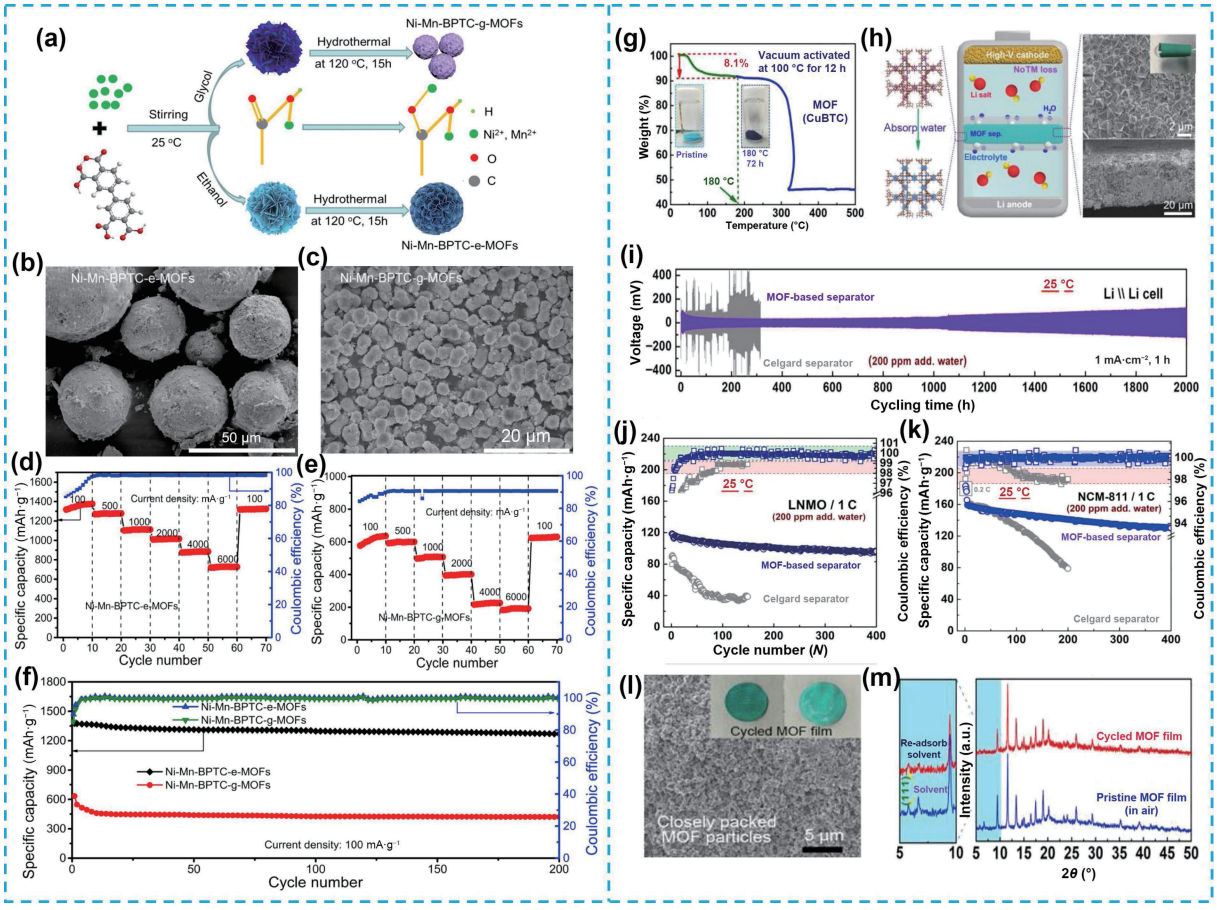

Figure 3 (a) Schematic of the synthesis of Ni-Mn-MOFs. SEM images of (b) Ni-Mn-BPTC-e-MOFs and (c) Ni-Mn-BPTC-g-MOFs. ((d) and (e)) Multiplicity properties. (f) Cycling properties. (g) TGA curves of MOFs. (h) The process of MOF inhibition by electrolyte water. (i) Electrochemical performance of MOF-based separator and Li/Li$^+$ symmetric batteries. ((j) and (k)) Cycling performance of Li//$LiNi_{0.5}Mn_{1.5}O_4$ batteries and Li//$LiNi_{0.8}Co_{0.1}Mn_{0.1}O_2$ batteries. (l) Pristine SEM image. Digital photographs of the pristine and cycled MOF diaphragm (inset). (m) X-ray diffraction (XRD) patterns of the MOFs water purifier before and after cycling. ((a)–(f)) Reproduced with permission from Ref. [105], © American Chemical Society 2020. ((g)–(m)) Reproduced with permission from Ref. [106], © The Royal Society of Chemistry 2020.

dendrites by enhancing the solid electrolyte interface (SEI) layer and equalizing the Li coating/exfoliation process [118–120].

A MOF based butaneditrile electrolyte was fabricated by Han et al. which can accelerate the transfer of lithium ion and alleviate the problem of lithium dendrites [121]. The porous structure of MOFs is first tuned to a suitable size. Then, the characteristic of the target electrolyte that permits the passage of only small-sized Li ions is used to direct the homogeneous Li ion transfer and alleviate the Li dendrite phenomenon. The successful preparation of the MOFs-SN-FEC (SN: succinonitrile, FEC: fluoroethylene carbonate) electrolyte after crushing and stamping the precursor ZIF-68 and heating is shown in Fig. 4(a). The LMBs with MOFs-SN-FEC as electrolyte exhibited excellent electrochemical performance due to the achievement of dendrite free Li deposition [123, 124]. The capacity retention was maintained at 98.9% at 0.1 C after 100 performance cycles in Fig. 4(b) [125, 126]. In addition, LMBs also exhibit good multiplicative performance, achieving a discharge capability of 140 mAh·g^{-1} at 1 C in Fig. 4(c) [127].

It is a widely accepted view in the scientific community that nature is full of intelligent ideas. Therefore, getting close to nature may lead to some unexpected inspiration in material design. A quasi-solid electrolyte inspired by the common tree in nature with a "trunk" form has been engineered for use in LMBs to increase service life [122, 128]. MOFs with a cellulose internal framework are designed as flexible electrolytes with excellent thermal stability and outstanding mechanical strength (Fig. 4(d)) [124]. The LMBs had long-term performance stability at 1 C under a cathode quality loading of 14.8 mg·cm^{-2} (Fig. 4(e)). The capacity retention was 80% after 300 long cycles, demonstrating good cycling performance (Fig. 4(f)) [129].

Modulation of ion transport (Li$^+$ and anions) in the vicinity of the lithium metal is another approach to solving the lithium dendrite problem. Mitigation of lithium dendrites by promoting lithium-ion mobilization and limiting anion transfer [123]. In addition, uniform lithium deposition likewise avoids the appearance of a large number of lithium dendrites. Using this method, researchers have successfully developed a functionalized diaphragm that can modulate ion transport by coating polypropylene (PP) diaphragms with MOFs in Fig. 4(g) [130]. LMBs with MOFs@PP diaphragms provide a greater discharge capacity of 139.24 mAh·g^{-1} at 0.1 C (Fig. 4(h)). Also, the capacity retention ratio is 98.08% after 50 cycles at 2 C, demonstrating excellent cycling stability (Fig. 4(i)) [131].

Although the dendritic growth of Li can be effectively suppressed by reinforcing SEI layer and homogenizing Li plating/stripping process, these strategies still cannot solve the problems of volume expansion of bulk lithium anode and large interface impedance of unmodified SEI [124]. Methods such as enhanced SEI layer and uniformized Li plating/peeling can inhibit the growth of Li dendrites to a certain extent. Nevertheless, these methods cannot fundamentally address the issues of volume expanding of lithium positive electrodes and high surface resistance of SEI interface in Fig. 4(j) [132]. The adopted open-architecture MOFs (OA-MOFs)/Cu@Li anode for LMBs achieves low voltage hysteresis and high-capacity retention at a high current density of 15 mA·cm^{-2} in Fig. 4(k) [133]. Persistent voltage

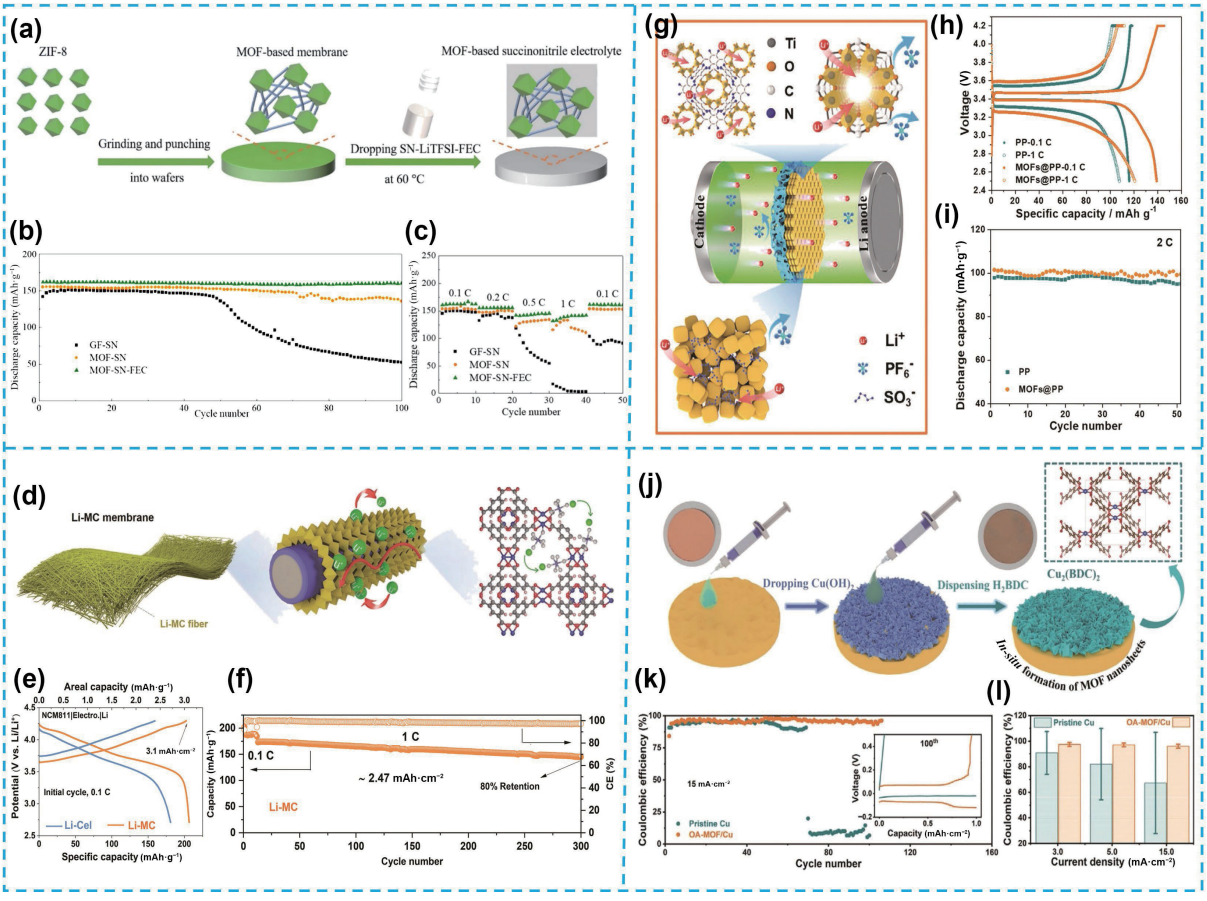

Figure 4 (a) Synthesis process of MOFs-SN-FEC electrolyte. (b) Cycling performance of MOFs-SN-FEC electrolyte-based batteries. (c) Multiplication performance at different multiplication rates. (d) Schematic diagram of Li-MOF/cellulose quasi-solid-state electrolyte (Li-MC QSSE). (e) Charge/discharge cycling curves. (f) Cycling performance curves at 1 C. (g) Schematic of the MOFs@PP separator. (h) Charge–discharge cycle curves at different rates. (i) Long charge–discharge performance cycle. (j) Schematic of the synthesis of OA-MOFs/Cu electrodes. (k) Coulombic efficiency of Li||Cu batteries. (l) Average Coulombic efficiency and standard deviation. ((a)–(c)) Reproduced with permission from Ref. [121], © American Chemical Society 2021. ((d)–(f)) Reproduced with permission from Ref. [122], © Wiley-VCH GmbH 2022. ((g)–(i)) Reproduced with permission from Ref. [123], © Wiley-VCH GmbH 2021. ((j)–(l)) Reproduced with permission from Ref. [132], © Wiley-VCH GmbH 2021.

curves of symmetric lithium batteries having minor overpotential in repetitive lithium plating/stripping procedures in Fig. 4(l).

3.2.1 *MOFs for LSBs*

With the growing demand for a better life, the need for high-capacity energy storage devices is also improving. For this reason, it is urgent to find suitable novel energy storage devices. Elemental sulfur has a variety of excellent properties, such as plentiful reserves, easy availability, low cost, environmental friendliness, and high theoretical capacity of 1675 mAh·g^{-1}. Consequently, LSBs are regarded as the most prospective rechargeable battery [134]. In fact, the application of LSBs is limited by the shuttle effect produced by the sulfur cathode and the lithium dendrites grown by the lithium metal anode, which hinders their widespread development. To solve this problem, researchers have successfully discovered that when porous materials are used as sulfur bodies, coatings or spacers, polysulfide migration can be inhibited to mitigate the shuttle effect; when porous materials are used as ionic sieves, Li^+ flux distribution can be adjusted to achieve uniform Li deposition and mitigate the effect of lithium dendrites [135]. MOFs with adjustable pore structure, structural versatility and functional multiplicity display enormous advantages in facilitating the rapid development of LSBs [136].

Amorphous MOFs were successfully synthesized by a simple ligand competition approach, exhibiting catalytic activity and high adsorption capacity for sulfur compounds owing to their undercoordination interaction [137]. Preparation of the desired cMIL-88B (c: crystalline) by a ligand competition process in which the amino group in the original cMIL-88B is replaced with 2-methylimidazole (2-MeIM, Fig. 5(a)). aMIL-88B (a: amorphous) have a bipyramidal hexagonal morphology, showing a round edge (Fig. 5(b)) [138–140]. The LSBs modified by aMIL-88B diaphragm achieve high efficiency and reversible sulfur electrochemistry and show excellent speed ability. aMIL-88B modification enables a great magnification performance up to 5 C (Fig. 5(c)) [138].

The construction of interlayered batteries structure between the cathode and separator can solve the challenge of polysulfide shuttle by providing good binding interactions with the polysulfides without bringing too much extra weight to the batteries. Carbon nano tubes and ferrocene-based two-dimensional (2D) MOF (Zr-Fc MOF) nanoflakes were prepared by facile vacuum filtration to prepare multi-functional interlayers (Zr-Fc MOFs/carbon nanotube (CNT)) [138]. Zr-Fc MOFs have excellent electrocatalytic effects on the redox kinetics of polysulfides. They also inhibit the shuttle effect for polysulfides by chemical anchoring capacity and electrostatic gravity (Fig. 5(d)) [141]. LSBs coupled with Zr-Fc MOFs CNT intercalation show enhanced rate performance and excellent cycling performance. The low-capacity decay rate reached 0.027% after 1500 cycles at 1 C with a sulfur loading of 4.11 mg·cm^{-2} (Fig. 5(e)) [142].

Based on the interlayer structure of the cathode/spacer/anode within the batteries, compared with the ordinary diaphragm, the functionalized separator can not only restrain the shuttle effect but also stabilize the lithium metal negative electrode [139]. The large number of Co-O_4 groups at the 2D MOFs-Co nanosheets can

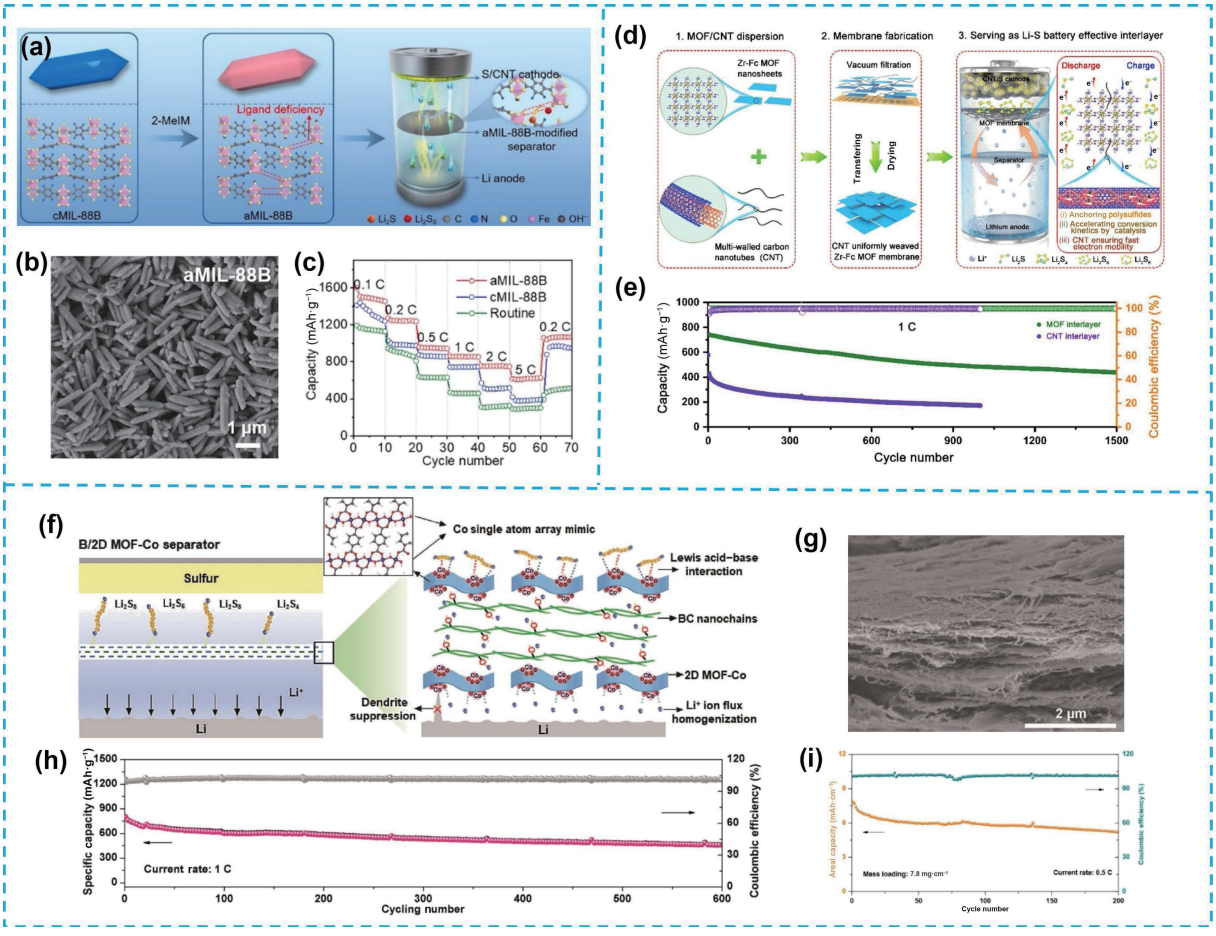

Figure 5 (a) Amorphization scheme of aMIL-88B and its application as a segregation modifier. (b) Scanning electron micrograph of aMIL-88B. (c) Magnification properties. (d) Schematic representation of Zr-Fc MOFs/CNT membranes and their use as an intercalation to immobilize polysulphides. (e) Cycle performance. (f) B/2D MOFs-Co separator. (g) SEM image of the B/2D MOFs-Co separator. (h) Long-term stability of LSBs at 1 C. (i) Cycling performance of LSBs at a sulfur loading of 7.8 mg·cm^{-2}. ((a)–(c)) Reproduced with permission from Ref. [137], © Elsevier Ltd. 2021. ((d) and (e)) Reproduced with permission from Ref. [138], © Elsevier B.V. 2021. ((f)–(i)) Reproduced with permission from Ref. [143], © Wiley-VCH 2020.

anchor polysulfides through Lewis acid-base interactions, allowing Li^+ to pass through uniformly and effectively inhibiting lithium dendrite growth and polysulfide diffusion in Fig. 5(f) [143]. An electron microscope scanning image through a near-surface cross-section of a B/2D MOFs-Co spacer trenchantly showing its layered microstructure in Fig. 5(g) LSBs based on bifunctional B/2D MOFs-Co spacers, which achieve long-term cycling performance. After up to 600 cycles, it still has 0.027% ultralow capacity decay in Fig. 5(h) [144]. Maintains an area capacity with 5.0 mAh·cm^{-2} over 200 cycles, despite a large sulfur loading up to 7.8 mg·cm^{-2} in Fig. 5(i) [145].

3D ordered macroporous MOFs (3DOM-MOFs) have great potential for application in energy storage and conversion, and have received extensive attention from researchers. This is a result of their distinctive structure that can accelerate ion dispersion and favorable structural stability [146–150]. Cui et al. successfully synthesized a new type of 3D organized large-pore MOF (3DOM ZIF-8) consisting of a large number of nanosized ZIF-8 subunits using a self-templated ligand duplication approach in Figs. 6(a) and 5(b) [151]. Under the condition of high load and limited electrolyte, a high area capacity of more than 6 mAh·cm^{-2} and decent cyclability are obtained, as shown in Figs. 6(c) and 6(d) [152].

π–d conjugated MOFs are a novel class of materials with potential for a wide range of applications, in which there is a conjugation of π-bonds and d-bonds between metal ions and ligands [147]. They possess good electrical conductivity, multiple redox centers, as well as low bulk change during cycling and stability associated with the delocalization of electrons. The π–d hybridization of Ni-MOFs-1D (1D: one-dimensional) provides a high density of off-domain electrons, and this conjugation enhances the electronic conductivity and catalytic activity of the material in Fig. 6(e). The capacity decay rate for S@Ni-MOFs-1D electrode is 0.018%, and the Coulombic efficiency is stable and more than 99.6% at 3 C for 1000 cycles in Fig. 6(f). Excellent multiplier performance of 575 mAh·g^{-1} was also obtained at 8 C in Fig. 6(g) [33]. A high-surface-area capacity at 6.63 mAh·cm^{-2} was obtained when the sulphur loading was 6.7 mg·cm^{-2} in Fig. 6(h) [153].

Stronger adsorption of lithium polysulphide by bimetallic organic framework compared to monometallic organic framework [148]. Homogeneous dispersion of Li_2S_x with sulfur-containing copper ions possessing high combining energy within Al-MOFs by hydrothermal method, and Al/Cu-MOFs bimetallic materials were prepared as advanced cathode materials in Fig. 6(i). Compared with the capacity provided by monometallic Al-MOFs, the bimetallic cathode material Al/Cu-MOFs-S obtained a higher preliminary capacity at 974.2 mAh·g^{-1} in Fig. 6(j) [154]. In addition, Al/Cu-MOFs-5-S exhibited a higher specific capacity than the Al-MOFs-S in Fig. 6(k) [155].

Conductive MOFs show significant potential for energy storage due to their excellent electronic conductivity and facilitated polysulfide transformation compared to conventional MOFs [149]. Ni-HHTP (HHTP: 2,3,6,7,10,11-hexahydroxytriphenylene) has good electronic conductivity, and can restore adsorbed polysulphides back into solid Li_2S, which improves active

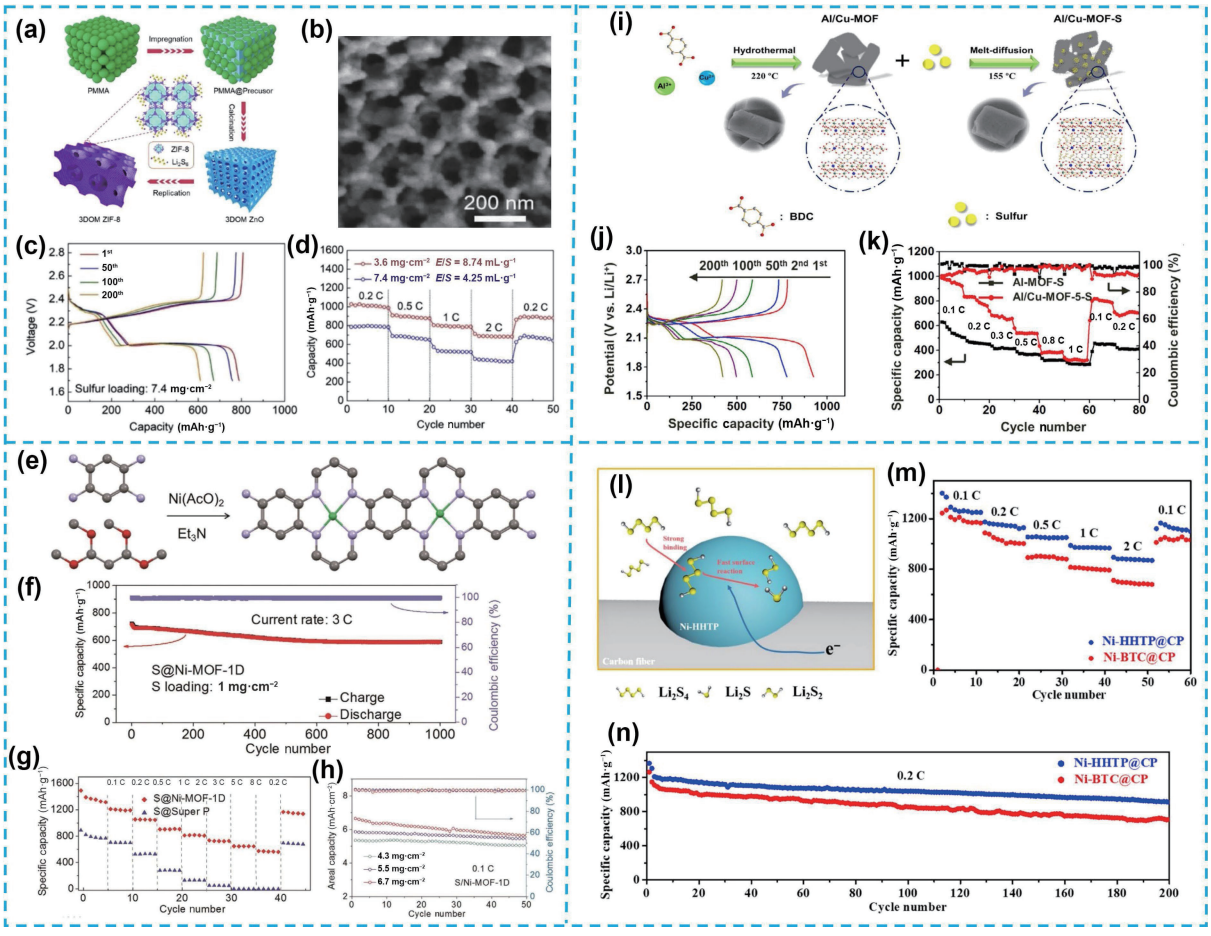

Figure 6 (a) Preparation process of 3DOM ZIF-8. (b) Transmission electron microscopy image of 3DOM ZIF-8. (c) The greatest common divisor (GCD) curve at 0.2 C. (d) Doubling performance. (e) Synthesis process of Ni-MOFs-1D. (f) Cycling stability. (g) Doubling performance of S@Ni-MOFs-1D and S@super P electrodes. (h) Highly loaded sulphur cycling performance. (i) Synthesis process of Al/Cu-MOFs-S. (j) GCD curve of Al/Cu-MOFs-5-S. (k) Doubling performance of Al-MOFs-S. (l) Process diagram of polysulphide reduction on Ni-HHTP@CP. (m) Doubling performance. (n) Cycling performance. ((a)–(d)) Reproduced with permission from Ref. [146], © Elsevier Ltd. 2020. ((e)–(h)) Reproduced with permission from Ref. [147], © Wiley-VCH GmbH 2022. ((i)–(k)) Reproduced with permission from Ref. [148], © Zhengzhou University 2021. ((l)–(n)) Reproduced with permission from Ref. [149], © Science Press and Dalian Institute of Chemical Physics, Chinese Academy of Sciences. Published by ELSEVIER B.V. and Science Press 2021.

substance availability for LSBs in Fig. 6(l). Compared to the Ni-BTC@CP (CP: carbon paper) batteries, the Ni-HHTP@CP-based LSBs provide an even better multiplicative performance at 2 C, reaching a capacity of 892 mAh·g^{-1} in Fig. 6(m) [156]. Furthermore, Ni-HHTP@CP has good cycling performance with an initial discharge capacity of up to 1366 mAh·g^{-1} in Fig. 6(n) [157].

3.2.2 *MOFs for LOBs*

Rechargeable LOBs featuring high energy density, high voltage and long-term cycle life have a broad range of potential applications in the domain of energy storage [158]. However, LOBs currently face a number of challenges, the main ones being the growth of lithium metal dendrites, degradation of the electrolyte and cathode materials and the reaction kinetics of the oxygen reduction reaction (ORR). These issues limit the lifetime of the batteries and require further research and improvement for commercial applications [159]. The electrochemical properties of LOBs are mainly determined by the structure of the cathode material [160]. MOFs have been tried as promising materials for LOBs catalysts and cathodes because of their porous structure, open active center, and adjustable pore size [161].

It is a brilliant concept to improve the long cycle performance of LOBs by designing efficient cathode materials. Compared with the single transition metal oxide electrode, the hybrid electrode can make use of the synergistic effect between the components to obtain better electrochemical performance [162]. A series of sword-shaped Co-MOFs layers were grown *in-situ* on carbon cloth (CC), which were subsequently macerated by addition of nickel nitrate solution, and finally thermolyzed at air to obtain freestanding Co_3O_4@$NiCo_2O_4$ sheet array cathode materials in Fig. 7(a) [163–165]. The Co_3O_4@$NiCo_2O_4$/CC cathode material exhibits outstanding electrochemical performance, obtaining the specific capacity as high as 10,645 mAh·g^{-1} and demonstrating a high capacity even after achieving more than 200 cycles in Figs. 7(b) and 7(c) [115, 166].

The design and synthesis of bifunctional catalysts with large specific surface area by MOFs on the nanometer scale can improve the performance of LOBs [163]. Dy-BTC (Dy: dysprosium) nanospheres are white powder with spherical rough surface under scanning electron microscope (SEM) in Fig. 7(d). Figure 7(e) illustrates the discharge/charging operation of a typical LOBs. Compared to the test batteries without Dy-BTC, the highest discharge capacity of LOBs with Dy-BTC nanospheres as cathode material was 3.5 times higher reaching 7618 mAh·g^{-1} in Fig. 7(f) [167, 168]. In addition, the cathode of Dy-BTC nanospheres obtained a discharge capacity at 1000 mAh·g^{-1} after 76 cycles at a current density of 200 mA·g^{-1}. This is clearly superior to the performance of massive crystal Dy-BTC, which has a lifetime of only 26 cycles in Fig. 7(g) [169].

The reversible deposition/decomposition of Li_2O_2 can be realized by high efficiency oxygen catalyst. It not only has high electrical conductivity of charge transfer, but also has high gas permeability of oxygen diffusion and high efficiency of catalysis to

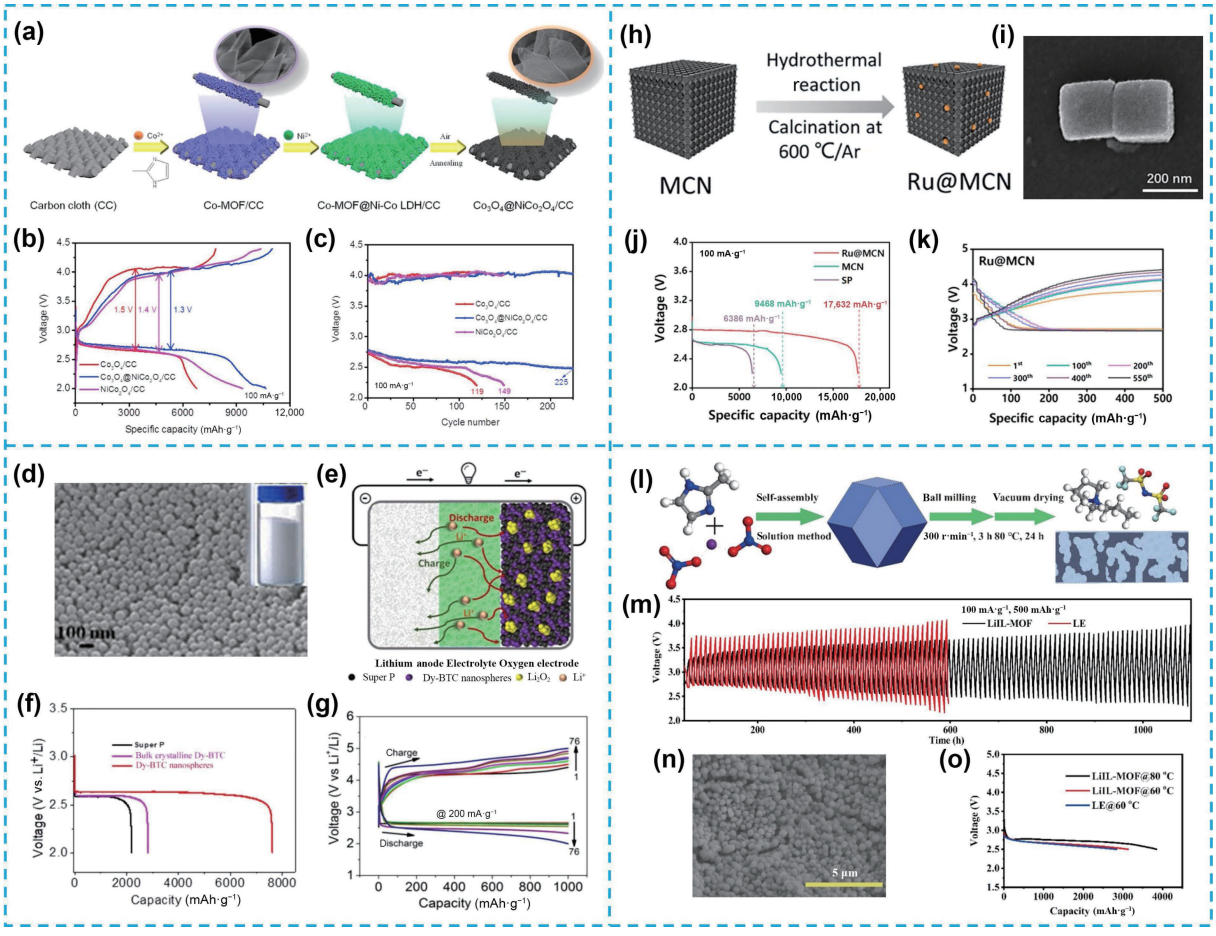

Figure 7 (a) Preparation process of Co_3O_4@$NiCo_2O_4$/CC cathode. (b) Initial charge/discharge curves. (c) Plot of terminal voltage as a function of the number of cycles. (d) SEM image of Dy-BTC nanospheres. (e) Working diagram of LOBs. (f) Initial discharge curves. (g) Representative cycling response at the limit of specific capacity of 1000 mAh·g^{-1}. (h) Synthetic map of Ru@MCN. (i) FE-SEM image of Ru@MCN. (g) Total specific capacity of discharge. (k) Charge–discharge curve. (l) Preparation process of quasi-solid LiIL-MOFs electrolyte. (m) Cycling performance. (n) SEM image after 100 cycles. (o) Deep discharge curve. ((a)–(c)) Reproduced with permission from Ref. [162], © Elsevier B.V. 2020. ((d)–(g)) Reproduced with permission from Ref. [163], © The Royal Society of Chemistry 2020. ((h)–(k)) Reproduced with permission from Ref. [164], © American Chemical Society 2021. ((l)–(o)) Reproduced with permission from Ref. [165], © American Chemical Society 2022.

reduce charge/discharge overpotentials [164]. Wei and colleagues managed to synthesis mesoporous copper nano-cubes possessing a high relative surface area, which were then compactly bound to ruthenium nano-particles to prepare oxygen cathode catalysts in Fig. 7(h) [170]. The SEM images show that Ru@MCN (MCN: mucinous cystic adenocarcinoma) has a cubic structure, which fully continues the morphological characteristics of the precursor in Fig. 7(i). The Ru@MCN-based LOBs obtained a gross specific discharge capacity of 17,632 mAh·g^{-1} at 100 mA·g^{-1}, which demonstrated better performance than the MCN and Super P batteries in Fig. 7(j). In addition, excellent cycling properties were demonstrated after more than 500 cycles at a current density of 1000 mA·g^{-1} in Fig. 7(k) [171, 172].

Liu et al. proposed a multifunctional semi-solid electrolyte to regulate ion migration for uniform lithium electrodeposition with MOFs and ionic liquids (ILs) [165]. The LiIL-MOFs electrolyte was prepared by a series of operations including grinding, stirring and vacuum heating in Fig. 7(l). The LOBs still work after 100 cycles, showing better cycling performance than the LES batteries in Fig. 7(m) [173]. The LiIL-MOFs electrolyte retained its complex properties after 100 cycles, indicating its structural stability in Fig. 7(n). The LOBs based on LiIL-MOFs show higher capacity than the LOBs based on LE at 60 and 80 °C in Fig. 7(o) [174].

3.3 MOFs for KIBs

KIBs have the advantages of simple battery design, low standard potentials, inexpensive materials and fabrication procedures, and fast ion transfer capability. KIBs are not only one of the main alternatives to LIBs, but also a research hotspot in energy storage technology [175–177]. KIBs possess significantly greater energy densities potentially due to a lower steady-state redox electric potential in K/K$^+$ [178]. The lower Lewis acidity and narrower ionic radius for K$^+$ give it ion mobility and high permittivity [179]. KIBs still face problems such as severe electrolyte decomposition during charging and discharging, dendrite growth, structural instability of the electrodes and poor heat dissipation, which have delayed their widespread application [180, 181]. MOF having unique characteristics can solve these problems to a large extent and facilitate the widespread promotion of KIBs in terms of market applications [182–184].

Deng et al. proposed a new type of low-cost microporous iron-based MOFs (MOFs-235) as the anode host of KIBs. A conventional solvothermal method was used to synthesise MOFs-235, which consists of a linear organic phthalate and hexahedral iron-based terpolymer with a periodic reticulated pore structure and a large pore capacity (Fig. 8(a)) [185]. The massive MOFs-235 exhibit a biconical bipyramid geometry with a particle size range of 200 nm up to 2 μm (Fig. 8(b)) [186]. After 200 long performance cycles, the reversible capacity of MOFs-235/MCNTs (MCNTs: multi-walled carbon nanotubes) reaches 132 mAh·g^{-1} with coulomb efficiency close to 100% (Fig. 8(c)) [187]. The stability of the crystal structure was demonstrated.

Under the condition of high temperature, the cycle stability of KIBs is poor. For this reason, Lu and co-workers designed a high

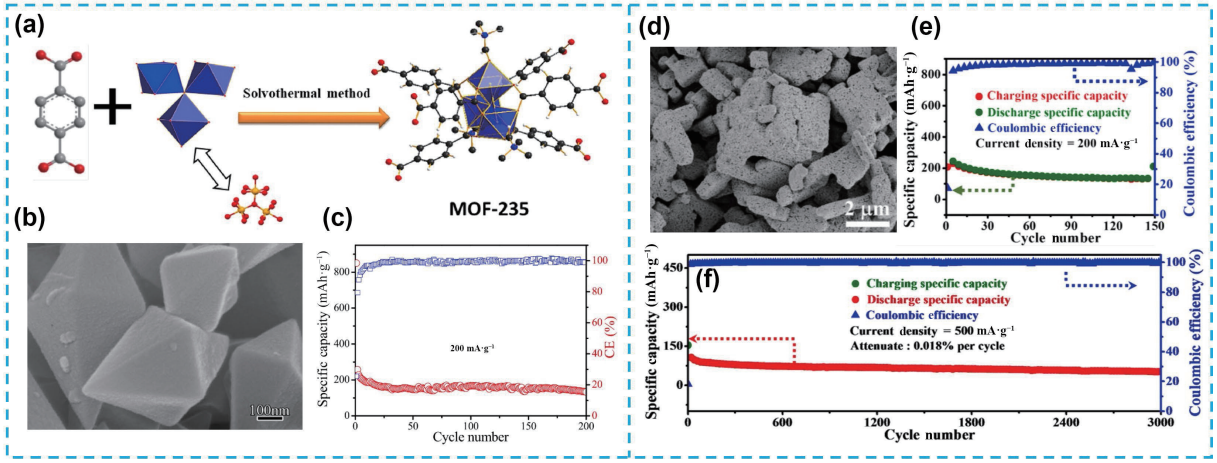

Figure 8 (a) Structural framework diagram of MOFs-235. (b) SEM image of MOFs-235. (c) Cycling performance at 200 mA·g^{-1}. (d) SEM image of 3MOFs-5. (e) Cycling performance. (f) Coulombic efficiency. ((a)–(c)) Reproduced with permission from Ref. [185], © Elsevier B.V. 2020. ((d)–(f)) Reproduced with permission from Ref. [188], © Elsevier B.V. 2021.

temperature KIBs with high stability using MOFs-5 as the anode materials [188]. As shown in Fig. 8(d), 3MOFs-5 consists of many small particles and has a large pore size, which facilitates ion transport to obtain excellent electrochemical performance. The primary discharge specific capacity of 3MOFs-5-based KIBs was 1183 mAh·g^{-1} at a current density of 200 mA·g^{-1} [189]. After up to 150 performance cycles, the KIBs still keep the specific capacity at 160 mAh·g^{-1}, demonstrating good cycling performance. In addition, it still obtains a highly reversible specific capacity with 56 mAh·g^{-1} at 500 mA·g^{-1}, representing a capacity retention rate of nearly 100%. Even after 3000 cycles, the decay per cycle is 0.018%, which demonstrates its stability in Figs. 8(e) and 8(f) [190].

3.4 MOFs for ZIBs

Rechargeable ZIBs are promising candidates in large-scale energy storage systems due to their high specific capacity, inherent safety, low cost and environmental friendliness [191]. Nevertheless, irreversible chemical reactions at the cathode and growth of zinc dendrites at the anode inevitably occur during long battery cycling, leading to deterioration of electrochemical performance [192, 193]. MOFs with tunable porous structural features provide convenient transport pathways and more reaction sites for rapid ion transport, resulting in increased battery capacity [194]. In addition, the special pore size of MOFs is more favorable for the dispersion of Zn^{2+} to ensure the sedimentation of Zn below the protective layer of MOFs. The controllable and diverse morphological features of MOFs are conducive to the formation of stable 2D films on the electrode surface [195].

Workers such as Yang inhibited zinc dendrite formation by adding a saturated electrolyte [196]. According to the fact that the saturated electrolyte system ("solvent in salt") is beneficial to the stability of the electrode, a new idea of developing a supersaturated electrolyte front surface through MOFs coating to obtain homogeneous zinc deposition is proposed. Mechanism of action of MOFs coatings to inhibit H_2O and build supersaturated front surfaces in Fig. 9(a). The capacity retention of naked zinc anode is 67.3% and the capacity retention of zinc anodes coated with MOFs is as high as 94.4% in Fig. 9(b) [197, 198]. The capacity of bare zinc anode attenuates rapidly and its cycle life is limited. As shown in Fig. 9(c), the structure of the zinc coating is smoother, the changes of surface pores and shape are negligible, and the electrodeposition of zinc shows a dense, dendritic-free pattern. As shown in Fig. 9(d), ZIBs obtained a specific capacity of 160.3 mAh·g^{-1} after 600 cycles, with a capacity retention rate of 88.9% [199].

Wang and co-workers solved the dendritic problem of zinc anodes by using a U-shaped deposition structure composed of 2D MOFs flake nanoarrays grown on zinc anodes [200]. This combination of pre-crystallization and bottom-up deposition removes the "tip effect" and suppresses Zn dendrites in Fig. 9(e). Porphyrin-based 2D MOFs nano-arrays, Zn-tetra-(4-carboxyphenyl) porphyrin (Zn-TCPP) were successfully synthesized by the self-templating approach in surfactant-free conditions in Fig. 9(f). Compared to the Zn//ZVO (ZVO: $Zn_xV_2O_5{\cdot}H_2O$) battery, the Zn-TCPP/Zn//ZVO battery Coulombic efficiency reaches 99.9%, showing better cycling stability in Fig. 9(g) [201, 202]. At current density of 5 mA·cm^{-2}, Zn-TCPP/Zn anodes obtained stability up to nearly 2000 h and low overpotential 50 mV in Fig. 9(h) [203–205].

Yin and co-workers propose coordination unsaturation approach to develop novel anode materials having rapid intercalation/deintercalation dynamics and favourable endurance [206]. A novel coordinated unsaturated Mn-MOF as a high-level cathode in ZIBs in Fig. 9(i). The appropriate unsaturated coordination degree ensures the efficient transport and electron exchange of zinc ions, thus ensuring the rapid electro-chemical reaction dynamics and the high-eigen activity in the process of repeated charge and discharge in Fig. 9(j) [207–209]. Mn-H_3BTC-MOFs-4-based ZIBs exhibited excellent batteries performance at a current density of 100 mV·g^{-1} with a discharge capacity for 138 mAh·g^{-1} in Fig. 9(k). At a current density of 3000 mA·g^{-1}, the capacity reached 93.5% from the original capacity upon cycling for 1000 cycles, demonstrating excellent long-cycle stability in Fig. 9(l) [210].

Manganese (BTC) cathodes and ZIF-8 coated zinc anodes achieve high-performance ZIB, solving the problems of fast capacity decay of cathode materials and instability of zinc anode retting/galvanising in Fig. 9(m) [211]. Mn(BTC) polymetallic oxide film has strong zinc storage capacity in Fig. 9(n), and the unique porous architecture within the ZIF-8 layer results in a homogeneous dezincification/electroplating of the zinc anode surface in Fig. 9(o) [212, 213]. In addition, the capacity retention rate is still above 90% after 900 performance cycles at a current density of 1000 mA·g^{-1}, indicating a good long cycle stability of the battery in Fig. 9(p) [214, 215].

3.5 MOFs for zinc-air batteries (ZABs)

ZABs are half-savings, half-fuel batteries with high theoretical energy density, low manufacturing cost, environmental friendliness, and high safety [216, 217]. The air cathode of ZABs is prone to severe polarisation resulting in a short lifetime. This limits the potential of ZABs and seriously affects their application

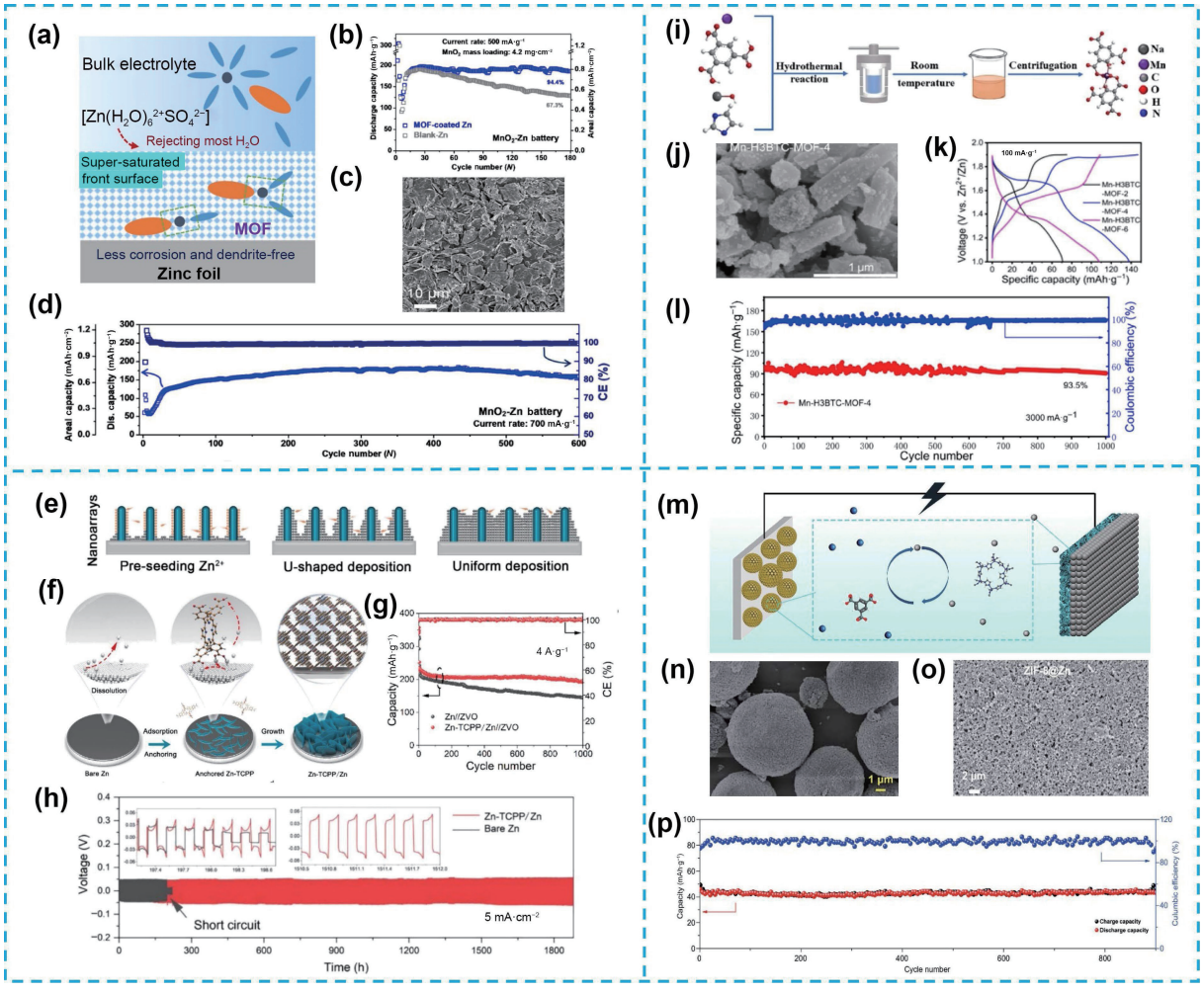

Figure 9 (a) Zn surface change process. (b) Cycling stability of MnO_2-Zn batteries. (c) SEM images of Zn in Zn anodes coated with MOFs. (d) Cycling stability and long-term cycling stability efficiency. (e) U-shaped Zn deposition on Zn substrate. (f) Synthesis process of Zn-TCPP/Zn. (g) Capacity retention and coulomb curves of Zn-TCPP/Zn//ZVO batteries. (h) Cycling performance. (I) Synthesis process of Mn-H_3BTC-MOFs-4. (j) SEM images of Mn-H_3BTC-MOFs-4. (k) Charge–discharge time profiles. (l) Cycling performance. (m) Mn(BTC)//ZIF-8@Zn. ((n) and (o)) SEM images of Mn(BTC) and ZIF-8@Zn. (p) Cycle performance. ((a)–(d)) Reproduced with permission from Ref. [196], © Wiley-VCH Verlag GmbH & Co. KGaA, Weinheim 2020. ((e)–(h)) Reproduced with permission from Ref. [200], © Elsevier B.V. 2022. ((i)–(l)) Reproduced with permission from Ref. [206], © American Chemical Society 2021. ((m)–(p)) Reproduced with permission from Ref. [211], © Pu, X. C. et al. 2020.

development and market promotion [218, 219]. In addition, zinc electrodes have a series of fatal drawbacks such as hydrogen precipitation corrosion, high self-discharge rate, inability to be recharged, and zinc dendrites leading to short circuits. This leads to the fact that ZABs cannot completely replace LIBs [220, 221]. MOFs-based bifunctional oxygen electrocatalysts can solve the problem of slow kinetics of ORR and oxygen evolution reaction (OER) at the air cathode of ZABs to a certain extent and accelerate the reaction efficiency. Their diverse structures, adjustable properties, and simple and easy-to-manufacture characteristics have led to great progress in the catalytic reverse side [222–224].

The organic molecular H_3BTC is highly engineered with a conjugated system, which has outstanding coordination with metal cations, and is therefore dedicated to promising features for bifunctional oxygen reactions catalysts [225]. Ni/Fe-BTC-MOFs was successfully prepared by cathodic electro-syntheses method using quantitative nickel chloride and ferric chloride as raw materials in Fig. 10(a). As shown in Fig. 10(b), the rod-like morphology of Ni/Fe-BTC-MOFs can be clearly seen in the field-emission SEM (FE-SEM) image. Ni/Fe-BTC-MOFs demonstrated outstanding cycling stability for over 594 h along with 5262 cycles in Fig. 10(c) without any important attenuation of the discharge–charge voltage [226, 227].

Li et al. designed and synthesized a family of Co and Fe hybridized MOFs (HCF-MOFs) which can be directly used as electrocatalysts [228]. HCF-MOFs-3 showed two different morphologies: 2D sheets integrated in the microspheres and nanoparticles scattered at the microsphere surface in Fig. 10(d). Its distinctive segregated construction offers a number of channels that not only accelerate ion transport but also ensure a high degree of exposed metal sites. This leads to increased electrocatalytic activity [229]. The activated HCF-MOFs in ZABs had a low over-potential with 295 mV and displayed good electrocatalytic OER potentials in Fig. 10(e). In addition, the ultimate current density in ORR was 4.99 mA·cm^{-2}, showing good electrochemical performance in Fig. 10(f). A final ultra-high-power density for 113.5 mW·cm^{-2} was obtained at 0.86 V and 100 mA·cm^{-2} in Fig. 10(g) [230].

3.6 MOFs for other batteries

In addition to the batteries introduced above, the application of MOFs in various types of batteries include zinc iodide (Zn-I_2) batteries, lithium selenium batteries, aluminum-sulphur batteries, nickel-zinc batteries and so on. The following is a brief introduction to zinc iodide batteries and lithium selenium batteries. Selenium has a high theoretical capacity, high conductivity and bulk capacity, and is regarded as a potential electrode material in lithium-selenium batteries [231, 232].

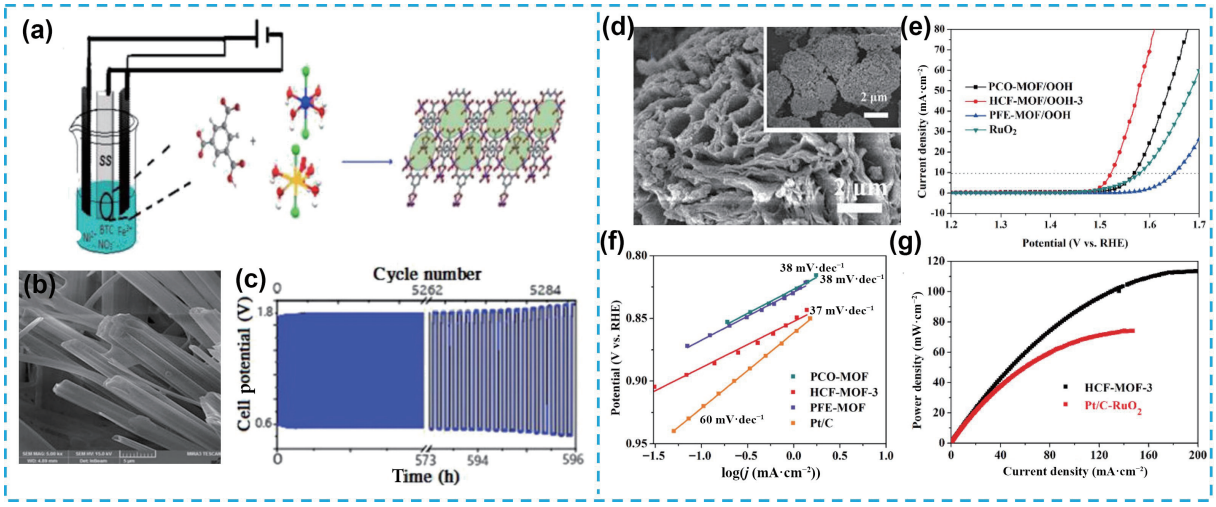

Figure 10 (a) Synthesis process of Ni/Fe-BTC MOFs thin-film nanotubes. (b) SEM images. (c) Charge/discharge cycling performance and round-trip efficiency. (d) SEM images of HCF-MOFs-3. (e) OER polarisation curves. (f) Tafel plots. (g) power density. ((a)–(c)) Reproduced with permission from Ref. [225], © Elsevier B.V. 2020. ((d)–(g)) Reproduced with permission from Ref. [228], © Wiley-VCH GmbH 2020.

However, polyselenide shuttling, polyselenide reaction with lithium electrode, and inhomogeneous Li^+ deposition can lead to poor stability of lithium-selenium batteries [233]. Selective primary care network (PCN) diaphragms can improve the performance of lithium-selenium batteries by inhibiting polyselenide shuttling and enhancing lithium-ion transport [234, 235]. Zinc-iodide batteries are a highly promising metal anode material for rechargeable aqueous batteries due to the large reserves of raw materials in the earth's crust, medium potential and high theoretical capacity [236]. However, the shuttle effect of triiodide and corrosion of zinc anodes due to side reactions, zinc-iodide batteries are unable to meet the market demand due to the limitation of service life [237–239]. Multifunctional MOF films can address these issues simultaneously within a certain range.

Shuttling of multi-selenium compounds leads to fast self-discharge, poor cycling stability, and poor Coulombic stability of lithium-selenium batteries, which impedes the adoption of lithium-selenium batteries. Cation-selective PCN-250 (Fe) separator applied to porous polypropylene membrane (PPM) not only inhibits the shuttle of polyselenium compounds but also improves Li^+ transmission in lithium-selenium batteries in Fig. 11(a) [231]. The SEM image of the cross-sectional area of the MOFs separator in Fig. 11(b) [234]. The lithium selenium batteries based on PCN diaphragm has excellent cycling stability, obtaining a reversible capacity for 423 $mAh·g^{-1}$ even after 100 cycles at 0.2 C. In addition, the Coulombic efficiency remained above 98% even after 500 performance cycles in Fig. 11(c) [235].

Zinc-iodine batteries are of interest because of their rich natural resources (0.0075% mass fraction Zn of earth crust) [236]. Nevertheless, the lifetime of Zn-I_2 batteries is very short, which seriously hinders its further development [237]. Zn-BTC multifunctional membrane designed by Yang et al. can effectively inhibit I^{3-} shuttling and parasitic secondary reactions at zinc electrodes in Fig. 11(d) [232]. The surface of the zinc anode was maintained smooth and compact with no obvious collapse of the structure, proving its cyclic stability in Fig. 11(e) [238]. The water-based Zn-I_2 batteries with Zn-BTC membrane achieve long life. A specific capacity of 85.1 $mAh·g^{-1}$ and a coulomb efficiency of up to 99.65% were obtained even after up to 6000 cycles in Fig. 11(f) [232].

4 Conclusion and perspective

This review summary on the synthesis for MOFs and their latest applications as electrode materials in various batteries. The synthesis method, morphological features and electrochemical properties of MOFs are highlighted. The structures show that MOFs materials have adjustable and diverse structural features,

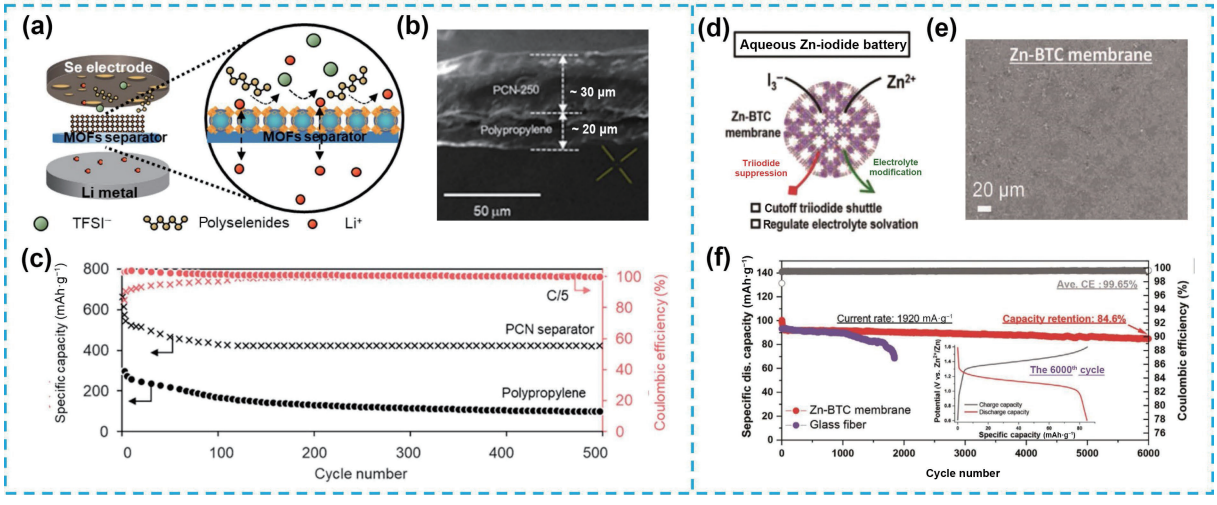

Figure 11 (a) MOFs spacer. (b) SEM image. (c) Period cycling performance. (d) Zn-BTC membrane-based battery. (e) SEM image after cycling. (f) Electrochemical performance. The insertion curves are charge/discharge curves. ((a)–(c)) Reproduced with permission from Ref. [231], © American Chemical Society 2021. ((d)–(f)) Reproduced with permission from Ref. [232], © Wiley-VCH GmbH 2020.

excellent mechanical properties, and good electrochemical properties, which make them a rare material for batteries. Compared with traditional batteries, the batteries (LIBs, LSBs, LOBs, KIBs, ZIBs, etc.) using MOFs as electrode materials have a great improvement in life and capacity. In recent years MOF has achieved great results in the direction of the battery field and has been widely promoted in the market. Although the application of MOFs in these batteries is a hot topic in energy storage, the safety risks caused by the digestion of electrolytes and cathodes, and the continuous growth of dendrites seriously affect the stability of batteries, which limits the application market of batteries in a wide range of fields. In order to meet the market demand and achieve greater research success, there are still some problems to be solved in this research field.

(1) The poor conductivity of MOFs needs to be further improved, which has a significant impact on the electron transport rate and reaction dynamics, which affects the application and development of MOFs in batteries to some extent. The electrical conductivity may be enhanced through composite of MOFs with some conductive materials. In addition, the method of coordinating atoms/groups of special nature or introducing structural stabilisers can further improve the conductivity or stability of MOFs.

(2) MOF materials improve the performance of the batteries to some extent, but the morphology will change in the process of charge and discharge. During the process, the reason for the change of MOF structure and the reaction mechanism to improve the electrochemical properties of the batteries are not clear. Adjusting and improving the components and architectural features of MOFs to prepare novel electrode materials with reversible reaction provides a certain assurance for exploiting the electrochemical reaction mechanism and identifying the activity center. At the same time, advanced *in-situ* testing and various characterisation techniques can provide some help in exploring the components of MOF, structural changes, and the chemical reaction mechanism of battery charging and discharging processes during scientific research.

(3) The electrochemical stability of MOFs is poor, irreversible decomposition or transformation into amorphous phase will occur during the charge–discharge cycle, and the frame will be destroyed. In addition, MOFs will disintegrate and collapse in water, acid and alkali environment. The stability of MOFs can be enhanced by adjusting the metal ions and ligands, improving the properties of MOFs materials, and creating structurally stable and reaction-reversible electrode materials. Introducing multiple metal centers or exposing more active sites during the design of MOFs to increase ORR and OER activity and thus improve stability.

(4) The problem of low productivity and high production cost of MOF materials is also one of the issues that constrain their widespread development. The productivity of MOFs can be improved by reducing the particle size to the nanometer level or constructing new layered nanostructures. This could be solved through the synthesis of MOFs from inexpensive feedstocks that are rich in natural resources or easy to extract.

(5) The high pore structure and large specific surface area of MOF sometimes bring bad structure, which is one of the reasons for low Coulombic efficiency and low energy density. In order to MOF materials have made more progress in electrochemistry, the overall electrochemical performance of the battery can be improved to a certain extent by adjusting the synergistic effect between MOF and battery components.

(6) Most of the MOF materials are synthesized in the laboratory, and the synthesis methods are not only complicated but also time-consuming. Therefore, there is still a need to design simple and effective synthesis methods for the large-scale production of MOFs, which can be improved to a large extent by selecting suitable ligands and metal ions purposely.

In summary, MOFs materials have an unimaginable potential for energy storage devices and significant progress has been made in a new generation of batteries. Novel methods for the synthesis of MOFs materials and various applications in batteries have been widely developed. In addition, the resulting MOF composites will further enhance the electrochemical performance of batteries by introducing functional materials. However, the synthesis process and electrochemical properties of MOFs still have many issues that need to be improved. However, we believe that based on this review helps to understand the controllability and regularity of MOFs, which can be rationally designed and optimised to produce high-performance batteries to meet the market demand and promote the rapid development of the battery field.

Acknowledgements

This work was supported by National Natural Science Foundation of China (No. U1904215), Natural Science Foundation of Jiangsu Province (No. BK20200044), and Changjiang scholars program of the Ministry of Education (No. Q2018270).

References

[1] Guo, S. J.; Xiao, Y. B.; Wang, J.; Ouyang, Y.; Li, X.; Deng, H. Y.; He, W. C.; Zeng, Q. H.; Zhang, W.; Zhang, Q. et al. Ordered structure of interlayer constructed with metal-organic frameworks improves the performance of lithium-sulfur batteries. *Nano Res.* **2021**, *14*, 4556–4562.

[2] Zhang, Y. J.; Li, J.; Zhao, W. Y.; Dou, H. L.; Zhao, X. L.; Liu, Y.; Zhang, B. W.; Yang, X. W. Defect-free metal-organic framework membrane for precise ion/solvent separation toward highly stable magnesium metal anode. *Adv. Mater.* **2022**, *34*, 2108114.

[3] Mehtab, T.; Yasin, G.; Arif, M.; Shakeel, M.; Korai, R. M.; Nadeem, M.; Muhammad, N.; Lu, X. Metal-organic frameworks for energy storage devices: Batteries and supercapacitors. *J. Energy Storage* **2019**, *21*, 632–646.

[4] Hua, Y.; Li, X. X.; Chen, C. Y.; Pang, H. Cobalt based metal-organic frameworks and their derivatives for electrochemical energy conversion and storage. *Chem. Eng. J.* **2019**, *370*, 37–59.

[5] Liu, J. J.; Song, X. Y.; Zhang, T.; Liu, S. Y.; Wen, H. R.; Chen, L. 2D conductive metal-organic frameworks: An emerging platform for electrochemical energy storage. *Angew. Chem., Int. Ed.* **2021**, *60*, 5612–5624.

[6] Wu, X. X.; Zhou, C.; Dong, C. X.; Shen, C. L.; Shuai, B. B.; Li, C.; Li, Y.; An, Q. Y.; Xu, X.; Mai, L. Polydopamine-assisted *in-situ* formation of dense MOF layer on polyolefin separator for synergistic enhancement of lithium-sulfur battery. *Nano Res.* **2022**, *15*, 8048–8055.

[7] Ding, L.; Zeng, M.; Wang, H.; Jiang, X. B. Synthesis of MIL-101-derived bimetal-organic framework and applications for lithium-ion batteries. *J. Mater. Sci.: Mater. Electron.* **2021**, *32*, 1778–1786.

[8] Wang, Y. Y.; Zhang, X. Q.; Zhou, M. Y.; Huang, J. Q. Mechanism, quantitative characterization, and inhibition of corrosion in lithium batteries. *Nano Res. Energy* **2023**, *2*, e9120046.

[9] Ahmed, S.; Shim, J.; Sun, H. J.; Rim, H. R.; Lee, H. K.; Park, G. Nickel decorated bimetallic catalysts derived from metal-organic frameworks as cathode materials for rechargeable zinc-air batteries. *Mater. Lett.* **2021**, *283*, 128781.

[10] Tong, Z. Q.; Kang, T. X.; Wu, Y.; Zhang, F.; Tang, Y. B.; Lee, C. S. Novel metastable Bi:Co and Bi:Fe alloys nanodots@carbon as anodes for high rate K-ion batteries. *Nano Res.* **2022**, *15*, 7220–7226.

[11] Li, Z. L.; Wang, S. X.; Shi, J. K.; Liu, Y.; Zheng, S. Y.; Zou, H. Q.; Chen, Y. L.; Kuang, W. X.; Ding, K.; Chen, L. Y. et al. A 3D interconnected metal-organic framework-derived solid-state electrolyte for dendrite-free lithium metal battery. *Energy Stor. Mater.* **2022**, *47*, 262–270.

[12] Liu, J. B.; Qiao, Z. S.; Xie, Q. S.; Peng, D. L.; Xie, R. J. Phosphorus-doped metal-organic framework-derived CoS_2 nanoboxes with improved adsorption-catalysis effect for Li-S batteries. *ACS Appl. Mater. Interfaces* **2021**, *13*, 15226–15236.
[13] Zhang, S. L.; Sun, L.; Fan, Q. N.; Zhang, F. L.; Wang, Z. J.; Zou, J. S.; Zhao, S. Y.; Mao, J. F.; Guo, Z. P. Challenges and prospects of lithium-CO_2 batteries. *Nano Res. Energy* **2022**, *1*, e9120001.
[14] Sun, F. C.; Chen, T. T.; Li, Q.; Pang, H. Hierarchical nickel oxalate superstructure assembled from 1D nanorods for aqueous nickel-zinc battery. *J. Colloid Interface Sci.* **2022**, *627*, 483–491.
[15] Wei, A. K.; Wang, L.; Li, Z. Metal-organic framework derived binary-metal oxide/MXene composite as sulfur host for high-performance lithium-sulfur batteries. *J. Alloys Compd.* **2022**, *899*, 163369.
[16] Ge, H. Y.; Feng, X. L.; Liu, D. P.; Zhang, Y. Recent advances and perspectives for Zn-based batteries: Zn anode and electrolyte. *Nano Res. Energy* **2023**, *2*, e9120039.
[17] Yang, Z. Q.; Zhu, J. P.; Tang, W. H.; Ding, Y. An Fe_2O_3/Mn_2O_3 nanocomposite derived from a metal-organic framework as an anode material for lithium-ion batteries. *ChemistrySelect* **2022**, *7*, e202203107.
[18] Nam, K. W.; Park, S. S.; dos Reis, R.; Dravid, V. P.; Kim, H.; Mirkin, C. A.; Stoddart, J. F. Conductive 2D metal-organic framework for high-performance cathodes in aqueous rechargeable zinc batteries. *Nat. Commun.* **2019**, *10*, 4948.
[19] Zhou, H. J.; Yang, H.; Yao, S. Y.; Jiang, L.; Sun, N. C.; Pang, H. Synthesis of 3D printing materials and their electrochemical applications. *Chin. Chem. Lett.* **2022**, *33*, 3681–3694.
[20] Wang, Q. P.; Guo, C.; He, J. P.; Yang, S.; Liu, Z. F.; Wang, Q. H. Fe_2O_3/C-modified Si nanoparticles as anode material for high-performance lithium-ion batteries. *J. Alloys Compd.* **2019**, *795*, 284–290.
[21] Liu, D.; Lu, B. B.; Pei, W. Y.; Gu, Z. Y.; Yang, J.; Wu, X. L.; Ma, J. F. A new polyoxometalate-resorcin[4]arene-based framework as an efficient anode material for lithium-ion batteries. *J. Alloys Compd.* **2020**, *835*, 155314.
[22] Gao, M. Q.; Wang, Z. Y.; Lek, D. G.; Wang, Q. Towards high power density aqueous redox flow batteries. *Nano Res. Energy* **2023**, *2*, e9120045.
[23] Zhang, P.; Wei, Y.; Zhou, S. J.; Soomro, R. A.; Jiang, M. C.; Xu, B. A metal-organic framework derived approach to fabricate *in-situ* carbon encapsulated Bi/Bi_2O_3 heterostructures as high-performance anodes for potassium ion batteries. *J. Colloid Interface Sci.* **2023**, *630*, 365–374.
[24] Wang, X. X.; Ge, L.; Lu, Q.; Dai, J.; Guan, D. Q.; Ran, R.; Weng, S. C.; Hu, Z. W.; Zhou, W.; Shao, Z. P. High-performance metal-organic framework-perovskite hybrid as an important component of the air-electrode for rechargeable Zn-air battery. *J. Power Sources* **2020**, *46*, 228377.
[25] Zhu, F. L.; Tao, Y. L.; Bao, H. F.; Wu, X. S.; Qin, C.; Wang, X. L.; Su, Z. M. Ferroelectric metal-organic framework as a host material for sulfur to alleviate the shuttle effect of lithium-sulfur battery. *Chem.—Eur. J.* **2020**, *26*, 13779–13782.
[26] Liu, Y. L.; Liu, X. Y.; Feng, L.; Shao, L. X.; Li, S. J.; Tang, J.; Cheng, H.; Chen, Z.; Huang, R.; Xu, H. C. et al. Two-dimensional metal-organic framework nanosheets: Synthesis and applications in electrocatalysis and photocatalysis. *ChemSusChem* **2022**, *15*, e202102603.
[27] Qin, X. L.; Huang, Y.; Wang, K.; Xu, T. T.; Wang, Y. L.; Liu, P. B.; Kang, Y.; Zhang, Y. Novel hierarchically porous Ti-MOFs/nitrogen-doped graphene nanocomposite served as high efficient oxygen reduction reaction catalyst for fuel cells application. *Electrochim. Acta* **2019**, *297*, 805–813.
[28] Tang, Y. J.; Zheng, S. S.; Cao, S.; Yang, F. Y.; Guo, X. T.; Zhang, S. T.; Xue, H. G.; Pang, H. Hollow mesoporous carbon nanospheres space-confining ultrathin nanosheets superstructures for efficient capacitive deionization. *J. Colloid Interface Sci.* **2022**, *626*, 1062–1069.
[29] Du, M.; Geng, P. B.; Pei, C. X.; Jiang, X. Y.; Shan, Y. Y.; Hu, W. H.; Ni, L. B.; Pang, H. High-entropy Prussian blue analogues and their oxide family as sulfur hosts for lithium-sulfur batteries. *Angew. Chem., Int. Ed.* **2022**, *61*, e202209350.
[30] Geng, P. B.; Du, M.; Wu, C. S.; Luo, T. X.; Zhang, Y.; Pang, H. PPy-constructed core–shell structures from MOFs for confining lithium polysulfides. *Inorg. Chem. Front.* **2022**, *9*, 2389–2394.
[31] Wu, Z. Z.; Adekoya, D.; Huang, X.; Kiefel, M. J.; Xie, J.; Xu, W.; Zhang, Q. C.; Zhu, D. B.; Zhang, S. Q. Highly conductive two-dimensional metal-organic frameworks for resilient lithium storage with superb rate capability. *ACS Nano* **2020**, *14*, 12016–12026.
[32] Ye, Z. Q.; Jiang, Y.; Li, L.; Wu, F.; Chen, R. J. Rational design of MOF-based materials for next-generation rechargeable batteries. *Nano-Micro Lett.* **2021**, *13*, 203.
[33] Qi, C.; Xu, L.; Wang, J.; Li, H. L.; Zhao, C. C.; Wang, L. N.; Liu, T. X. Titanium-containing metal-organic framework modified separator for advanced lithium-sulfur batteries. *ACS Sustain. Chem. Eng.* **2020**, *8*, 12968–12975.
[34] Zhang, F. P.; Chen, L.; Zhang, Y. L.; Peng, Y. Y.; Luo, X.; Xu, Y. S.; Shi, Y. L. Engineering Co/CoO heterojunctions stitched in mulberry-like open-carbon nanocages via a metal-organic frameworks *in-situ* sacrificial strategy for performance-enhanced zinc-air batteries. *Chem. Eng. J.* **2022**, *447*, 137490.
[35] Zhang, Y. T.; Zhu, J.; Liu, Z. Y.; Li, S. B.; Huang, H.; Jiang, B. X. Microwave-assisted synthesis of Zr-based metal-organic polyhedron: Serving as efficient visible-light photocatalyst for Cr(VI) reduction. *Inorg. Chim. Acta* **2022**, *543*, 121204.
[36] Azbell, T. J.; Pitt, T. A.; Bollmeyer, M. M.; Cong, C.; Lancaster, K. M.; Milner, P. J. Ionothermal synthesis of metal-organic frameworks using low-melting metal salt precursors. *Angew. Chem., Int. Ed.* **2023**, *62*, e202218252.
[37] Bashar, B. S.; Kareem, H. A.; Hasan, Y. M.; Ahmad, N.; Alshehri, A. M.; Al-Majdi, K.; Hadrawi, S. K.; Al Kubaisy, M. M. R.; Qasim, M. T. Application of novel Fe_3O_4/Zn-metal organic framework magnetic nanostructures as an antimicrobial agent and magnetic nanocatalyst in the synthesis of heterocyclic compounds. *Front. Chem.* **2022**, *10*, 1014731.
[38] Zhou, J. J.; Liu, H.; Lin, Y. C.; Zhou, C.; Huang, A. S. Synthesis of well-shaped and high-crystalline Ce-based metal organic framework for CO_2/CH_4 separation. *Microporous Mesoporous Mater.* **2020**, *302*, 110224.
[39] Skoda, D.; Kazda, T.; Hanulikova, B.; Cech, O.; Vykoukal, V.; Michalicka, J.; Cudek, P.; Kuritka, I. Vanadium metal-organic frameworks derived VO_x/carbon nano-sheets and paperclip-like VO_x/nitrogen-doped carbon nanocomposites for sodium-ion battery electrodes. *Mater. Chem. Phys.* **2022**, *278*, 125584.
[40] Yuan, R. R.; He, H. M. Constructing a 3D porous Co(II)-organic framework: Synthesis, characterization and chemical transformation of epoxide and CO_2 into cyclic carbonate. *Inorg. Chem. Commun.* **2020**, *121*, 108235.
[41] Abo El-Yazeed, W. S.; Abou El-Reash, Y. G.; Elatwy, L. A.; Ahmed, A. I. Novel bimetallic Ag-Fe MOF for exceptional Cd and Cu removal and 3,4-dihydropyrimidinone synthesis. *J. Taiwan Inst. Chem. Eng.* **2020**, *114*, 199–210.
[42] Shan, Y.; Zhang, G. X.; Yin, W.; Pang, H.; Xu, Q. Recent progress in Prussian blue/Prussian blue analogue-derived metallic compounds. *Bull. Chem. Soc. Jpn.* **2022**, *95*, 230–260.
[43] Abánades Lázaro, I.; Mazarakioti, E. C.; Andres-Garcia, E.; Vieira, B. J. C.; Waerenborgh, J. C.; Vitórica-Yrezábal, I. J.; Giménez-Marqués, M.; Mínguez Espallargas, G. Ultramicroporous iron-isonicotinate MOFs combining size-exclusion kinetics and thermodynamics for efficient CO_2/N_2 gas separation. *J. Mater. Chem. A* **2023**, *11*, 5320–5327.
[44] Lee, G.; Yoon, J. H.; Kwon, K.; Han, H.; Song, J. H.; Lim, K. S.; Lee, W. R. Dimensional selective syntheses of metal-organic frameworks using mixed organic ligands. *Inorg. Chim. Acta* **2020**, *513*, 119739.
[45] Shah, R.; Ali, S.; Ali, S.; Xia, P. F.; Raziq, F.; Adnan; Mabood, F.; Shah, S.; Zada, A.; Ismail, P. M. et al. Amino functionalized metal-organic framework/RGO composite electrode for flexible Li-ion batteries. *J. Alloys Compd.* **2023**, *936*, 168183.
[46] Guo, X. T.; Li, W. T.; Geng, P. B.; Zhang, Q. Y.; Pang, H.; Xu, Q.

Construction of SiO_x/nitrogen-doped carbon superstructures derived from rice husks for boosted lithium storage. *J. Colloid Interface Sci.* **2022**, *606*, 784–792.
[47] He, S. H.; Li, Z. P.; Wang, J. Q. Bimetallic MOFs with tunable morphology: Synthesis and enhanced lithium storage properties. *J. Solid State Chem.* **2022**, *307*, 122726.
[48] Hou, J. M.; Guo, Y. P.; Zhang, Y. R.; Li, J. Z.; Xu, Y. P.; Fang, Z. X.; Yang, J.; Wu, M. Q. Facile green and sustainable synthesis of MnO@rGO as electrochemically stable anode for lithium-ion batteries. *Mater. Lett.* **2022**, *325*, 132761.
[49] Wang, M. X. Tremella-like NiO/$NiCo_2O_4$ nanocomposites as excellent anodes for cyclable lithium-ion batteries. *J. Cryst. Growth* **2022**, *589*, 126685.
[50] Li, T.; Tong, Y. H.; Li, J. W.; Kong, Z.; Liu, X. X.; Xu, H. Y.; Xu, H.; Wang, K. L.; Jin, H. *Hericium erinaceus*-like copper-based MOFs as anodes for high performance lithium-ion batteries. *ACS Appl. Energy Mater.* **2021**, *4*, 11400–11407
[51] Huang, K. S.; Li, B.; Zhao, M. M.; Qiu, J. Q.; Xue, H. G.; Pang, H. Synthesis of lithium metal silicates for lithium ion batteries. *Chin. Chem. Lett.* **2017**, *28*, 2195–2206.
[52] Choi, D.; Lim, S.; Han, D. Advanced metal-organic frameworks for aqueous sodium-ion rechargeable batteries. *J. Energy Chem.* **2021**, *53*, 396–406.
[53] Zhou, J. E.; Zhong, H.; Zhang, Y. Z.; Huang, Q. H.; Zhang, B. H.; Zeb, A.; Xu, Z. G.; Lin, X. M. An oxygen-deficient strategy to boost lithium storage of metal-organic framework-derived $ZnTiO_3/TiO_2$/C composite anodes. *Chem. Eng. J.* **2022**, *450*, 137448.
[54] Liu, H.; Zhao, Y. Y.; Zhou, C.; Mu, B.; Chen, L. Microwave-assisted synthesis of Zr-based metal-organic framework (Zr-fum-fcu-MOF) for gas adsorption separation. *Chem. Phys. Lett.* **2021**, *780*, 138906.
[55] Li, Q. L.; Liu, Y. B.; Niu, S. Y.; Li, C. H.; Chen, C.; Liu, Q. Q.; Huo, J. Microwave-assisted rapid synthesis and activation of ultrathin trimetal-organic framework nanosheets for efficient electrocatalytic oxygen evolution. *J. Colloid Interface Sci.* **2021**, *603*, 148–156.
[56] Wang, W. J.; Sun, Z. H.; Chen, S. C.; Qian, J. F.; He, M. Y.; Chen, Q. Microwave-assisted fabrication of a mixed-ligand $[Cu_4(\mu_3\text{-}OH)_2]$-cluster-based metal-organic framework with coordinatively unsaturated metal sites for carboxylation of terminal alkynes with carbon dioxide. *Appl. Organomet. Chem.* **2021**, *35*, e6288.
[57] Skoda, D.; Kazda, T.; Munster, L.; Hanulikova, B.; Styskalik, A.; Eloy, P.; Debecker, D. P.; Vyroubal, P.; Simonikova, L.; Kuritka, I. Microwave-assisted synthesis of a manganese metal-organic framework and its transformation to porous MnO/carbon nanocomposite utilized as a shuttle suppressing layer in lithium-sulfur batteries. *J. Mater. Sci.* **2019**, *54*, 14102–14122.
[58] Jiang, L. L.; Zeng, X. Z.; Li, M. K.; Wang, M. Q.; Su, T. Y.; Tian, X. C.; Tang, J. Rapid electrochemical synthesis of HKUST-1 on indium tin oxide. *RSC Adv.* **2017**, *7*, 9316–9320.
[59] Vo, T. K.; Le, V. N.; Quang, D. T.; Song, M.; Kim, D.; Kim, J. Rapid defect engineering of UiO-67 (Zr) via microwave-assisted continuous-flow synthesis: Effects of modulator species and concentration on the toluene adsorption. *Microporous Mesoporous Mater.* **2020**, *306*, 110405.
[60] González, L.; Gil-San-Millán, R.; Navarro, J. A. R.; Maldonado, C. R.; Barea, E.; Carmona, F. J. Green synthesis of zirconium MOF-808 for simultaneous phosphate recovery and organophosphorus pesticide detoxification in wastewater. *J. Mater. Chem. A* **2022**, *10*, 19606–19611.
[61] Appelhans, L. N.; Hughes, L.; McKenzie, B.; Rodriguez, M.; Griego, J.; Briscoe, J.; Moorman, M.; Frederick, E.; Wright, J. B. Facile microwave synthesis of zirconium metal-organic framework thin films on gold and silicon and application to sensor functionalization. *Microporous Mesoporous Mater.* **2021**, *323*, 111133.
[62] da Trindade, L. G.; Zanchet, L.; Dreon, R.; Souza, J. C.; Assis, M.; Longo, E.; Martini, E. M. A.; Chiquito, A. J.; Pontes, F. M. Microwave-assisted solvothermal preparation of Zr-BDC for modification of proton exchange membranes made of SPEEK/PBI blends. *J. Mater. Sci.* **2020**, *55*, 14938–14952.
[63] Salahdin, O. D.; Patra, I.; Ansari, M. J.; Emad Izzat, S.; Uktamov, K. F.; Abid, M. K.; Mahdi, A. B.; Hammid, A. T.; Mustafa, Y. F.; Sharma, H. Synthesis of efficient cobalt-metal organic framework as reusable nanocatalyst in the synthesis of new 1,4-dihydropyridine derivatives with antioxidant activity. *Front. Chem.* **2022**, *10*, 932902.
[64] Hu, L.; Wang, Q. S.; Zhu, X. D.; Meng, T.; Huang, B. B.; Yang, J. D.; Lin, X. M.; Tong, Y. X. Novel Fe_4-based metal-organic cluster-derived iron oxides/S,N dual-doped carbon hybrids for high-performance lithium storage. *Nanoscale* **2021**, *13*, 716–723.
[65] Vaitsis, C.; Kanellou, E.; Pandis, P. K.; Papamichael, I.; Sourkouni, G.; Zorpas, A. A.; Argirusis, C. Sonochemical synthesis of zinc adipate metal-organic framework (MOF) for the electrochemical reduction of CO_2: MOF and circular economy potential. *Sustain. Chem. Pharm.* **2022**, *29*, 100786.
[66] Yu, K.; Lee, Y. R.; Seo, J. Y.; Baek, K. Y.; Chung, Y. M.; Ahn, W. S. Sonochemical synthesis of Zr-based porphyrinic MOF-525 and MOF-545: Enhancement in catalytic and adsorption properties. *Microporous Mesoporous Mater.* **2021**, *316*, 110985.
[67] Beamish-Cook, J.; Shankland, K.; Murray, C. A.; Vaqueiro, P. Insights into the mechanochemical synthesis of MOF-74. *Cryst. Growth Des.* **2021**, *21*, 3047–3055.
[68] Cindro, N.; Tireli, M.; Karadeniz, B.; Mrla, T.; Užarević, K. Investigations of thermally controlled mechanochemical milling reactions. *ACS Sustain. Chem. Eng.* **2019**, *7*, 16301–16309.
[69] Wu, D. N.; Li, X. C.; Zheng, J.; He, C. J.; Zhang, J.; Xie, Y. R.; Li, Y. F.; Tang, B. H. J.; Rui, Y. C.; Liu, F. J. Self-healable metal-organic gel membranes as anodes with high lithium storage. *Electrochim. Acta* **2021**, *386*, 138334.
[70] Li, L.; Wang, Q. M.; Zhang, X. Y.; Fang, L. D.; Li, X. T.; Zhang, W. M. Unique three-dimensional Co_3O_4@N-CNFs derived from ZIFs and bacterial cellulose as advanced anode for sodium-ion batteries. *Appl. Surf. Sci.* **2020**, *508*, 145295.
[71] Xia, S. B.; Huang, W. J.; Shen, X.; Liu, J. M.; Cheng, F. X.; Guo, H.; Liu, J. J. Fabrication of porous Ni/$CoFe_2O_4$@C composite for pseudocapacitive lithium storage. *J. Alloys Compd.* **2021**, *854*, 157177.
[72] Liu, Y. Y.; Sun, K.; Jiang, J. C.; Zhou, W. S.; Shang, Y.; Du, C. X.; Li, B. J. Metallurgical pyrolysis toward Co@nitrogen-doped carbon composite for lithium storage. *Green Energy Environ.* **2021**, *6*, 91–101.
[73] Xue, Y. S.; Cheng, W. W.; Luo, X. M.; Cao, J. P.; Xu, Y. Multifunctional polymolybdate-based metal-organic framework as an efficient catalyst for the CO_2 cycloaddition and as the anode of a lithium-ion battery. *Inorg. Chem.* **2019**, *58*, 13058–13065.
[74] Chen, Y. Y.; Chen, J. H.; Liu, J. W.; Lin, Z.; Hu, X.; Lin, X. M.; Xu, Z. G.; Zeb, A. Metal-organic framework-derived mixed-phase anatase/rutile TiO_2 towards boosted lithium storage: Surface engineering and design strategy through crystal phase transition. *Mater. Today Nano* **2022**, *20*, 100265.
[75] Mallarabanavadi Ravikumar, M.; Rajshekar Shetty, V.; Suresh, G. S. Synthesis and applications of aurin tricarboxylic acid-copper metal organic framework for rechargeable lithium-ion batteries. *J. Electrochem. Soc.* **2020**, *167*, 100533.
[76] Cui, X.; Liang, M. X.; Wang, L.; Li, L. G.; Peng, Q. Q.; Dong, H. H.; Qi, S.; Sun, W. W.; Lv, L. P.; Chen, X. F. et al. High structural stability and reaction mechanism of porous carbon nanobox encapsulated monodisperse CoP nanoparticles for high-performance lithium-ion battery. *Batter. Supercaps* **2022**, *5*, e202200271.
[77] Hu, W. H.; Zheng, M. B.; Duan, H. Y.; Zhu, W.; Wei, Y.; Zhang, Y.; Pan, K. M.; Pang, H. Heat treatment-induced Co^{3+} enrichment in CoFePBA to enhance OER electrocatalytic performance. *Chin. Chem. Lett.* **2022**, *33*, 1412–1416.
[78] Shi, X.; Lin, X. J.; Liu, S. T.; Li, A.; Chen, X. H.; Zhou, J. S.; Ma, Z. K.; Song, H. H. Flake-like carbon coated Mn_2SnO_4 nanoparticles as anode material for lithium-ion batteries. *Chem. Eng. J.* **2019**, *372*, 269–276.

[79] Gao, X. Y.; Zhu, G.; Zhang, X. J.; Hu, T. Porous carbon materials derived from *in situ* construction of metal-organic frameworks for high-performance sodium ions batteries. *Microporous Mesoporous Mater.* **2019**, *273*, 156–162.

[80] Li, J. P.; Li, Y. J.; Ma, X. D.; Zhang, K.; Hu, J. H.; Yang, C. H.; Liu, M. L. A honeycomb-like nitrogen-doped carbon as high-performance anode for potassium-ion batteries. *Chem. Eng. J.* **2020**, *384*, 123328.

[81] Fan, L.; Guo, X. T.; Hang, X. X.; Pang, H. Synthesis of truncated octahedral zinc-doped manganese hexacyanoferrates and low-temperature calcination activation for lithium-ion battery. *J. Colloid Interface Sci.* **2022**, *607*, 1898–1907.

[82] Fang, Y. X.; Chen, Y. L.; Zeng, L. X.; Yang, T.; Xu, Q. X.; Wang, Y. Y.; Zeng, S. H.; Qian, Q. R.; Wei, M. D.; Chen, Q. H. Nitrogen-doped carbon encapsulated zinc vanadate polyhedron engineered from a metal-organic framework as a stable anode for alkali ion batteries. *J. Colloid Interface Sci.* **2021**, *593*, 251–265.

[83] Gu, S.; Liu, D. N.; Zhang, X.; Huang, H.; Zhang, Y. L.; Cheng, Z. Q.; Liu, Q.; Meng, L. Q.; Wang, J. H.; Chu, P. K. et al. Finite phosphorene derived partial reduction of metal organic framework nanofoams for enhanced lithium storage capability. *J. Power Sources* **2022**, *525*, 231025.

[84] Li, N.; Guo, X. W.; Tang, X. R.; Xing, Y. C.; Pang, H. Three-dimensional $Co_2V_2O_7{\cdot}nH_2O$ superstructures assembled by nanosheets for electrochemical energy storage. *Chin. Chem. Lett.* **2022**, *33*, 462–465.

[85] Furukawa, H.; Miller, M. A.; Yaghi, O. M. Independent verification of the saturation hydrogen uptake in MOF-177 and establishment of a benchmark for hydrogen adsorption in metal-organic frameworks. *J. Mater. Chem.* **2007**, *17*, 3197–3204.

[86] Li, X. X.; Cheng, F. Y.; Zhang, S. N.; Chen, J. Shape-controlled synthesis and lithium-storage study of metal-organic frameworks Zn_4O(1,3,5-benzenetribenzoate)$_2$. *J. Power Sources* **2006**, *160*, 542–547.

[87] Yu, L. T.; Zhang, L. G.; Fu, J. J.; Yun, J. M.; Kim, K. H. Hierarchical Tiny-Sb encapsulated in MOFs derived-carbon and TiO_2 hollow nanotubes for enhanced Li/Na-ion half-and full-cell batteries. *Chem. Eng. J.* **2021**, *417*, 129106.

[88] Liu, X. F.; Guo, X. Q.; Wang, R.; Liu, Q. C.; Li, Z. J.; Zang, S. Q.; Mak, T. C. W. Manganese cluster-based MOF as efficient polysulfide-trapping platform for high-performance lithium-sulfur batteries. *J. Mater. Chem. A* **2019**, *7*, 2838–2844.

[89] Yuan, Y. F.; Chen, F.; Ye, L. W.; Cai, G. S.; Zhu, M.; Yin, S. M.; Guo, S. Y. Construction of Co_3O_4@TiO_2 heterogeneous mesoporous hollow nanocage-in-nanocage from metal-organic frameworks with enhanced lithium storage properties. *J. Alloys Compd.* **2019**, *790*, 814–821.

[90] Chen, L.; Yang, W. J.; Li, X. Y.; Han, L. J.; Wei, M. D. Co_9S_8 Embedded into N/S doped carbon composites: *In situ* derivation from a sulfonate-based metal-organic framework and its electrochemical properties. *J. Mater. Chem. A* **2019**, *7*, 10331–10337.

[91] Zheng, S. S.; Ru, Y.; Xue, H. G.; Pang, H. Fluorinated pillared-layer metal-organic framework microrods for improved electrochemical cycling stability. *Chin. Chem. Lett.* **2021**, *32*, 3817–3820.

[92] Wu, N.; Yang, Y. J.; Jia, T.; Li, T. H.; Li, F.; Wang, Z. Sodium-tin metal-organic framework anode material with advanced lithium storage properties for lithium-ion batteries. *J. Mater. Sci.* **2020**, *55*, 6030–6036.

[93] Manthiram, A. An outlook on lithium ion battery technology. *ACS Cent. Sci.* **2017**, *3*, 1063–1069.

[94] Li, C.; Zhang, C.; Xie, J.; Wang, K. B.; Li, J. Z.; Zhang, Q. C. Ferrocene-based metal-organic framework as a promising cathode in lithium-ion battery. *Chem. Eng. J.* **2021**, *404*, 126463.

[95] Mutahir, S.; Wang, C. X.; Song, J. J.; Wang, L.; Lei, W.; Jiao, X. Y.; Khan, M. A.; Zhou, B. J.; Zhong, Q.; Hao, Q. L. Pristine Co(BDC)TED$_{0.5}$ a pillared-layer biligand cobalt based metal organic framework as improved anode material for lithium-ion batteries. *Appl. Mater. Today* **2020**, *21*, 100813.

[96] Jiang, Y. C.; Zhao, H. T.; Yue, L. C.; Liang, J.; Li, T. S.; Liu, Q.; Luo, Y. L.; Kong, X. Z.; Lu, S. Y.; Shi, X. F. et al. Recent advances in lithium-based batteries using metal organic frameworks as electrode materials. *Electrochem. Commun.* **2021**, *122*, 106881.

[97] Song, J. J.; He, B.; Wang, X. C.; Guo, Y. Q.; Peng, C. Q.; Wang, Y.; Su, Z.; Hao, Q. L. Hollow porous nanocuboids cobalt-based metal-organic frameworks with coordination defects as anode for enhanced lithium storage. *J. Mater. Sci.* **2021**, *56*, 17178–17190.

[98] Peng, Y.; Bai, Y.; Liu, C. L.; Cao, S.; Kong, Q. Q.; Pang, H. Applications of metal-organic framework-derived N,P,S doped materials in electrochemical energy conversion and storage. *Coord. Chem. Rev.* **2022**, *466*, 214602.

[99] Zheng, W.; Bi, W. Y.; Gao, X. N.; Zhang, Z. G.; Yuan, W. H.; Li, L. A nickel and cobalt bimetal organic framework with high capacity as an anode material for lithium-ion batteries. *Sustain. Energy Fuels* **2020**, *4*, 5757–5764.

[100] Rambabu, D.; Lakraychi, A. E.; Wang, J. D.; Sieuw, L.; Gupta, D.; Apostol, P.; Chanteux, G.; Goossens, T.; Robeyns, K.; Vlad, A. An electrically conducting Li-ion metal-organic framework. *J. Am. Chem. Soc.* **2021**, *143*, 11641–11650.

[101] Wu, X. Y.; Ru, Y.; Bai, Y.; Zhang, G. X.; Shi, Y. X.; Pang, H. PBA composites and their derivatives in energy and environmental applications. *Coord. Chem. Rev.* **2022**, *451*, 214260.

[102] Wang, Z. K.; Bi, R.; Liu, J. D.; Wang, K. B.; Mao, F. F.; Wu, H.; Bu, Y. Q.; Song, N. H. Polyoxometalate-based Cu/Zn-MOFs with diverse stereo dimensions as anode materials in lithium ion batteries. *Chem. Eng. J.* **2021**, *404*, 127117.

[103] Gao, C. W.; Jiang, Z. J.; Qi, S. B.; Wang, P. X.; Jensen, L. R.; Johansen, M.; Christensen, C. K.; Zhang, Y. F.; Ravnsbæk, D. B.; Yue, Y. Z. Metal-organic framework glass anode with an exceptional cycling-induced capacity enhancement for lithium-ion batteries. *Adv. Mater.* **2022**, *34*, 2110048.

[104] Dai, Z. X.; Long, Z. W.; Li, R. R.; Shi, C.; Qiao, H.; Wang, K. L.; Liu, K. Metal-organic framework-structured porous $ZnCo_2O_4$/C composite nanofibers for high-rate lithium-ion batteries. *ACS Appl. Energy Mater.* **2020**, *3*, 12378–12384.

[105] Yin, C. J.; Xu, L. F.; Pan, Y. S.; Pan, C. L. Metal-organic framework as anode materials for lithium-ion batteries with high capacity and rate performance. *ACS Appl. Energy Mater.* **2020**, *3*, 10776–10786.

[106] Chang, Z.; Qiao, Y.; Deng, H.; Yang, H. J.; He, P.; Zhou, H. S. A stable high-voltage lithium-ion battery realized by an in-built water scavenger. *Energy Environ. Sci.* **2020**, *13*, 1197–1204.

[107] Panda, D. K.; Maity, K.; Palukoshka, A.; Ibrahim, F.; Saha, S. Li^+ ion-conducting sulfonate-based neutral metal-organic framework. *ACS Sustain. Chem. Eng.* **2019**, *7*, 4619–4624.

[108] Zhou, X. Y.; Yu, Y. W.; Yang, J.; Wang, H.; Jia, M.; Tang, J. J. Cross-linking tin-based metal-organic frameworks with encapsulated silicon nanoparticles: High-performance anodes for lithium-ion batteries. *ChemElectroChem* **2019**, *6*, 2056–2063.

[109] Wang, J.; Kong, F. J.; Chen, J. Y.; Han, Z. S.; Tao, S.; Qian, B.; Jiang, X. F. Metal-organic-framework-derived $FeSe_2$@carbon embedded into nitrogen-doped graphene sheets with binary conductive networks for rechargeable batteries. *ChemElectroChem* **2019**, *6*, 2805–2811.

[110] Zhang, J.; Zhou, L.; Sun, Q. J.; Ming, H.; Sun, L. S.; Wang, C. L.; Wu, Y. Q.; Guan, K.; Wang, L. M.; Ming, J. Metal-organic coordination strategy for obtaining metal-decorated Mo-based complexes: Multi-dimensional structural evolution and high-rate lithium-ion battery applications. *Chem.—Eur. J.* **2019**, *25*, 8813–8819.

[111] Xu, H. J.; Wang, L.; Zhong, J.; Wang, T.; Cao, J. H.; Wang, Y. Y.; Li, X. Q.; Fei, H. L.; Zhu, J.; Duan, X. D. Ultra-stable and high-rate lithium ion batteries based on metal-organic framework-derived In_2O_3 nanocrystals/hierarchically porous nitrogen-doped carbon anode. *Energy Environ. Mater.* **2020**, *3*, 177–185.

[112] Yang, Z.; Wang, J.; Wu, H. T.; Kong, F. J.; Yin, W. Y.; Cheng, H. J.; Tang, X. Y.; Qian, B.; Tao, S.; Yi, J. et al. MOFs derived $Co_{1-x}S$ nanoparticles embedded in N-doped carbon nanosheets with improved electrochemical performance for lithium ion batteries. *Appl. Surf. Sci.* **2019**, *479*, 693–699.

[113] Wang, Y. L.; Song, J.; Wong, W. Y. Constructing 2D sandwich-like MOF/MXene heterostructures for durable and fast aqueous zinc-ion batteries. *Angew. Chem., Int. Ed.* **2022**, *62*, e202218343.
[114] Yan, Z. L.; Liu, J. Y.; Lin, Y. F.; Deng, Z.; He, X. Q.; Ren, J. G.; He, P.; Pang, C. L.; Xiao, C. M.; Yang, D. R. et al. Metal-organic frameworks-derived CoMOF-D@Si@C core–shell structure for high-performance lithium-ion battery anode. *Electrochim. Acta* **2021**, *390*, 138814.
[115] Palani, R.; Wu, Y. S.; Wu, S. H.; Jose, R.; Yang, C. C. Metal-organic framework-derived ZrO_2/$NiCo_2O_4$/graphene mesoporous cake-like structure as enhanced bifunctional electrocatalytic cathodes for long life Li-O_2 batteries. *Electrochim. Acta* **2022**, *412*, 140147.
[116] Jiang, Y.; Shen, L. X.; Ma, H. T.; Ma, J. L.; Yang, K.; Geng, X. D.; Zhang, H. W.; Liu, Q. L.; Zhu, N. A low-strain metal organic framework for ultra-stable and long-life sodium-ion batteries. *J. Power Sources* **2022**, *541*, 231701.
[117] Jin, W. W.; Zou, J. Z.; Zeng, S. Z.; Inguva, S.; Xu, G. Z.; Li, X. H.; Peng, M.; Zeng, X. R. Tailoring the structure of clew-like carbon skeleton with 2D Co-MOF for advanced Li-S cells. *Appl. Surf. Sci.* **2019**, *469*, 404–413.
[118] Liu, Z. C.; Wang, D.; Mu, H. L.; Zhang, C. J.; Wu, L. Q.; Feng, L.; Sun, X. Y.; Zhang, G. S.; Wu, J.; Wen, G. W. Nanosized monometallic selenides heterostructures implanted into metal organic frameworks-derived carbon for efficient lithium storage. *J. Alloys Compd.* **2021**, *884*, 161151.
[119] Liu, K. Y.; Meng, X. H.; Yan, L. J.; Fan, M. Q.; Wu, Y. C.; Li, C.; Ma, T. L. Sn/SnO_x core–shell structure encapsulated in nitrogen-doped porous carbon frameworks for enhanced lithium storage. *J. Alloys Compd.* **2022**, *896*, 163009.
[120] Li, L.; Luo, Y. H.; Wang, Y. N.; Zhang, Z. S.; Wu, F. C.; Li, J. D. Rational design of a well-aligned metal-organic framework nanopillar array for superior lithium-sulfur batteries. *Chem. Eng. J.* **2023**, *454*, 140043.
[121] Han, D. D.; Wang, P. F.; Li, P.; Shi, J.; Liu, J.; Chen, P. J.; Zhai, L. P.; Mi, L. W.; Fu, Y. Z. Homogeneous and fast Li-ion transport enabled by a novel metal-organic-framework-based succinonitrile electrolyte for dendrite-free Li deposition. *ACS Appl. Mater. Interfaces* **2021**, *13*, 52688–52696.
[122] Zheng, Y.; Yang, N.; Gao, R.; Li, Z. Q.; Dou, H. Z.; Li, G. R.; Qian, L. T.; Deng, Y. P.; Liang, J. Q.; Yang, L. X. et al. "Tree-trunk" design for flexible quasi-solid-state electrolytes with hierarchical ion-channels enabling ultralong-life lithium-metal batteries. *Adv. Mater.* **2022**, *34*, 2203417
[123] Hao, Z. D.; Wu, Y.; Zhao, Q.; Tang, J. D.; Zhang, Q. Q.; Ke, X. X.; Liu, J. B.; Jin, Y. H.; Wang, H. Functional separators regulating ion transport enabled by metal-organic frameworks for dendrite-free lithium metal anodes. *Adv. Funct. Mater.* **2021**, *31*, 2102938.
[124] Li, D. X.; Wang, J.; Guo, S. J.; Xiao, Y. B.; Zeng, Q. H.; He, W. C.; Gan, L. Y.; Zhang, Q.; Huang, S. M. Molecular-scale interface engineering of metal-organic frameworks toward ion transport enables high-performance solid lithium metal battery. *Adv. Funct. Mater.* **2020**, *30*, 2003945.
[125] Li, Z. J.; Liu, Q. Q.; Gao, L. N.; Xu, Y. F.; Kong, X. Q.; Luo, Y.; Peng, H. X.; Ren, Y. R.; Wu, H. B. Quasi-solid electrolyte membranes with percolated metal-organic frameworks for practical lithium-metal batteries. *J. Energy Chem.* **2021**, *52*, 354–360.
[126] Jiang, X. B.; Shao, M. Y.; Li, K.; Ding, L.; Zeng, M. Facile synthesis and lithium storage mechanism study of directly usable tin-based metal organic framework. *J. Electroanal. Chem.* **2022**, *912*, 116268.
[127] Zhou, D.; Ni, J. F.; Li, L. Self-supported multicomponent CPO-27 MOF nanoarrays as high-performance anode for lithium storage. *Nano Energy* **2019**, *57*, 711–717.
[128] Chen, G. L.; Li, Y. J.; Zhong, W. T.; Zheng, F. H.; Hu, J. H.; Ji, X. H.; Liu, W. Z.; Yang, C. H.; Lin, Z.; Liu, M. L. MOFs-derived porous Mo_2C-C nano-octahedrons enable high-performance lithium-sulfur batteries. *Energy Stor. Mater.* **2020**, *25*, 547–554.
[129] Liu, L.; Sun, C. W. Flexible quasi-solid-state composite electrolyte membrane derived from a metal-organic framework for lithium-metal batteries. *ChemElectroChem* **2020**, *7*, 707–715.
[130] Zhu, X. Y.; Chang, Z.; Yang, H. J.; Qian, Y. M.; He, P.; Zhou, H. S. Sifting weakly-coordinated solvents within solvation sheath through an electrolyte filter for high-voltage lithium-metal batteries. *Energy Stor. Mater.* **2022**, *44*, 360–369.
[131] Liu, Y.; Liu, Q. Q.; Hong, Y. R.; Xu, Y. F.; Chen, Z. R.; Zhao, W.; Hu, Z. K.; Wang, J. W.; Wu, H. B. Solvent sieving separators implement dual electrolyte for high-voltage lithium-metal batteries. *Nano Res.* **2023**, *16*, 4901–4907.
[132] Wu, Q. P.; Zheng, Y. J.; Guan, X.; Xu, J.; Cao, F. H.; Li, C. L. Dynamical SEI reinforced by open-architecture MOF film with stereoscopic lithiophilic sites for high-performance lithium-metal batteries. *Adv. Funct. Mater.* **2021**, *31*, 2101034.
[133] Chen, D. C.; Mukherjee, S.; Zhang, C.; Li, Y.; Xiao, B. B.; Singh, C. V. Two-dimensional square metal organic framework as promising cathode material for lithium-sulfur battery with high theoretical energy density. *J. Colloid Interface Sci.* **2022**, *613*, 435–446.
[134] Park, J. S.; Kim, J. H.; Yang, S. J. Rational design of metal-organic framework-based materials for advanced Li-S batteries. *Bull. Korean Chem. Soc.* **2021**, *42*, 148–158.
[135] Wu, H.; Yang, Y. Q.; Jia, W.; Xiao, R.; Wang, H. Z. Defect-engineered bilayer MOFs separator for high stability lithium-sulfur batteries. *J. Alloys Compd.* **2021**, *874*, 159917.
[136] Bo, R. H.; Taheri, M.; Liu, B. R.; Ricco, R.; Chen, H. J.; Amenitsch, H.; Fusco, Z.; Tsuzuki, T.; Yu, G. H.; Ameloot, R. et al. Hierarchical metal-organic framework films with controllable meso/macroporosity. *Adv. Sci.* **2020**, *7*, 2002368.
[137] Zhang, X. M.; Li, G. R.; Zhang, Y. G.; Luo, D.; Yu, A. P.; Wang, X.; Chen, Z. W. Amorphizing metal-organic framework towards multifunctional polysulfide barrier for high-performance lithium-sulfur batteries. *Nano Energy* **2021**, *86*, 106094.
[138] Wang, Y.; Deng, Z.; Huang, J. Y.; Li, H. J.; Li, Z. Y.; Peng, X. S.; Tian, Y.; Lu, J. G.; Tang, H. C.; Chen, L. X. et al. 2D Zr-Fc metal-organic frameworks with highly efficient anchoring and catalytic conversion ability towards polysulfides for advanced Li-S battery. *Energy Stor. Mater.* **2021**, *36*, 466–477
[139] Jin, G. F.; Zhang, J. L.; Dang, B. Y.; Wu, F. C.; Li, J. D. Engineering zirconium-based metal-organic framework-801 films on carbon cloth as shuttle-inhibiting interlayers for lithium-sulfur batteries. *Front. Chem. Sci. Eng.* **2022**, *16*, 511–522.
[140] Li, C.; Zhang, X. F.; Zhang, Q.; Xiao, Y. H.; Fu, Y. Y.; Tan, H. H.; Liu, J. Q.; Wu, Y. C. Theoretical understanding for anchoring effect of MOFs for lithium-sulfur batteries. *Comput. Theor. Chem.* **2021**, *1196*, 113110.
[141] Yao, M. J.; Wang, R.; Zhao, Z. F.; Liu, Y.; Niu, Z. Q.; Chen, J. A flexible all-in-one lithium-sulfur battery. *ACS Nano* **2018**, *12*, 12503–12511.
[142] Zheng, Z. J.; Ye, H.; Guo, Z. P. Recent progress on pristine metal/covalent-organic frameworks and their composites for lithium-sulfur batteries. *Energy Environ. Sci.* **2021**, *14*, 1835–1853.
[143] Li, Y. J.; Lin, S. Y.; Wang, D. D.; Gao, T. T.; Song, J. W.; Zhou, P.; Xu, Z. K.; Yang, Z. H.; Xiao, N.; Guo, S. J. Single atom array mimic on ultrathin MOF nanosheets boosts the safety and life of lithium-sulfur batteries. *Adv. Mater.* **2020**, *32*, 1906722.
[144] Dang, B. Y.; Gao, D. Y.; Luo, Y. H.; Zhang, Z. S.; Li, J. D.; Wu, F. C. Bifunctional design of cerium-based metal-organic framework-808 membrane modified separator for polysulfide shuttling and dendrite growth inhibition in lithium-sulfur batteries. *J. Energy Storage* **2022**, *52*, 104981.
[145] Zhou, C.; Li, Z. H.; Xu, X.; Mai, L. Q. Metal-organic frameworks enable broad strategies for lithium-sulfur batteries. *Natl. Sci. Rev.* **2021**, *8*, nwab055.
[146] Benítez, A.; Amaro-Gahete, J.; Esquivel, D.; Romero-Salguero, F. J.; Morales, J.; Caballero, Á. MIL-88A metal-organic framework as a stable sulfur-host cathode for long-cycle Li-S batteries. *Nanomaterials* **2020**, *10*, 424.
[147] Yang, D. W.; Liang, Z. F.; Tang, P. Y.; Zhang, C. Q.; Tang, M. X.; Li, Q. Z.; Biendicho, J. J.; Li, J. S.; Heggen, M.; Dunin-Borkowski, R. E. et al. A high conductivity 1D π–d conjugated metal-organic

framework with efficient polysulfide trapping-diffusion-catalysis in lithium-sulfur batteries. *Adv. Mater.* **2022**, *34*, 2108835.
[148] Geng, P. B.; Du, M.; Guo, X. T.; Pang, H.; Tian, Z. Q.; Braunstein, P.; Xu, Q. Bimetallic metal-organic framework with high-adsorption capacity toward lithium polysulfides for lithium-sulfur batteries. *Energy Environ. Mater.* **2022**, *5*, 599–607.
[149] Wang, S.; Huang, F. Y.; Zhang, Z. F.; Cai, W. B.; Jie, Y. L.; Wang, S. Y.; Yan, P. F.; Jiao, S. H.; Cao, R. G. Conductive metal-organic frameworks promoting polysulfides transformation in lithium-sulfur batteries. *J. Energy Chem.* **2021**, *63*, 336–343.
[150] Li, Q.; Zhang, Y. F.; Zhang, G. X.; Wang, Y. X.; Pang, H. Recent advances in the development of perovskite@metal-organic frameworks composites. *Natl. Sci. Open* **2023**, *2*, 20220065.
[151] Cui, G. L.; Li, G. R.; Luo, D.; Zhang, Y. G.; Zhao, Y.; Wang, D. R.; Wang, J. Y.; Zhang, Z.; Wang, X.; Chen, Z. W. Three-dimensionally ordered macro-microporous metal organic frameworks with strong sulfur immobilization and catalyzation for high-performance lithium-sulfur batteries. *Nano Energy* **2020**, *72*, 104685.
[152] Qi, X. H.; Cai, D.; Wang, X. L.; Xia, X. H.; Gu, C. D.; Tu, J. P. Ionic liquid-impregnated ZIF-8/polypropylene solid-like electrolyte for dendrite-free lithium-metal batteries. *ACS Appl. Mater. Interfaces* **2022**, *14*, 6859–6868.
[153] Rana, M.; Al-Fayaad, H. A.; Luo, B.; Lin, T.; Ran, L. B.; Clegg, J. K.; Gentle, I.; Knibbe, R. Oriented nanoporous MOFs to mitigate polysulfides migration in lithium-sulfur batteries. *Nano Energy* **2020**, *75*, 105009.
[154] Chu, Z. H.; Gao, X. C.; Wang, C. Y.; Wang, T. Y.; Wang, G. X. Metal-organic frameworks as separators and electrolytes for lithium-sulfur batteries. *J. Mater. Chem. A* **2021**, *9*, 7301–7316.
[155] Chang, Z.; Qiao, Y.; Wang, J.; Deng, H.; He, P.; Zhou, H. S. Fabricating better metal-organic frameworks separators for Li-S batteries: Pore sizes effects inspired channel modification strategy. *Energy Stor. Mater.* **2020**, *25*, 164–171.
[156] Chang, Z.; Qiao, Y.; Wang, J.; Deng, H.; Zhou, H. S. Two-dimensional metal-organic framework with perpendicular one-dimensional nano-channel as precise polysulfide sieves for highly efficient lithium-sulfur batteries. *J. Mater. Chem. A* **2021**, *9*, 4870–4879.
[157] Parse, H. B.; Patil, I.; Kakade, B.; Swami, A. Cobalt nanoparticles encapsulated in N-doped carbon on the surface of MXene (Ti_3C_2) play a key role for electroreduction of oxygen. *Energy Fuels* **2021**, *35*, 17909–17918.
[158] Majidi, L.; Ahmadiparidari, A.; Shan, N. N.; Kumar Singh, S.; Zhang, C. J.; Huang, Z. H.; Rastegar, S.; Kumar, K.; Hemmat, Z.; Ngo, A. T. et al. Nanostructured conductive metal organic frameworks for sustainable low charge overpotentials in Li-air batteries. *Small* **2022**, *18*, 2102902.
[159] Zhan, Y.; Yu, S. Z.; Luo, S. H.; Feng, J.; Wang, Q. Nitrogen-coordinated CoS_2@NC yolk–shell polyhedrons catalysts derived from a metal-organic framework for a highly reversible Li-O_2 battery. *ACS Appl. Mater. Interfaces* **2021**, *13*, 17658–17667.
[160] Zhao, Y. J.; Ding, L.; Wang, X. M.; Yang, X. M.; He, J. B.; Yang, B. J.; Wang, B. N.; Zhang, D. W.; Li, Z. W. Yolk–shell ZIF-8@ZIF-67 derived Co_3O_4@$NiCo_2O_4$ catalysts with effective electrochemical properties for Li-O_2 batteries. *J. Alloys Compd.* **2021**, *861*, 157945.
[161] Guo, S. Q.; Sun, Y. X.; Wang, J. N.; Peng, L. C.; Li, H. Y.; Li, C. J. Bimetallic ZIF-derived cobalt nanoparticles anchored on N- and S-codoped porous carbon nanofibers as cathode catalyst for Li-O_2 batteries. *Electrochim. Acta* **2022**, *418*, 140279.
[162] Li, J.; Deng, Y. J.; Leng, L. M.; Liu, M. R.; Huang, L. L.; Tian, X. L.; Song, H. Y.; Lu, X. Y.; Liao, S. J. MOF-templated sword-like Co_3O_4@$NiCo_2O_4$ sheet arrays on carbon cloth as highly efficient Li-O_2 battery cathode. *J. Power Sources* **2020**, *450*, 227725.
[163] Liu, D.; Zhang, X. M.; Wang, Y. J.; Song, S. Y.; Cui, L. F.; Fan, H. B.; Qiao, X. C.; Fang, B. Z. A new perspective of lanthanide metal-organic frameworks: Tailoring Dy-BTC nanospheres for rechargeable Li-O_2 batteries. *Nanoscale* **2020**, *12*, 9524–9532.
[164] Wei, L.; Ma, Y.; Gu, Y. T.; Yuan, X. Z.; He, Y.; Li, X. J.; Zhao, L.; Peng, Y.; Deng, Z. Ru-embedded highly porous carbon nanocubes derived from metal-organic frameworks for catalyzing reversible Li_2O_2 formation. *ACS Appl. Mater. Interfaces* **2021**, *13*, 28295–28303.
[165] Liu, H. X.; Zhao, L. Y.; Xing, Y.; Lai, J. N.; Li, L.; Wu, F.; Chen, N.; Chen, R. J. Enhancing the long cycle performance of Li-O_2 batteries at high temperatures using metal-organic framework-based electrolytes. *ACS Appl. Energy Mater.* **2022**, *5*, 7185–7191.
[166] Wang, X. X.; Du, D. Y.; Xu, H. Y.; Yan, Y.; Wen, X. J.; Ren, L. F.; Shu, C. Z. NiMn-based metal-organic framework with optimized e_g orbital occupancy as efficient bifunctional electrocatalyst for lithium-oxygen batteries. *Chem. Eng. J.* **2023**, *452*, 139524.
[167] Zhao, G. Y.; Liu, Y. F.; Tang, L.; Zhang, L.; Sun, K. N. Capacitive behavior based on the ultrafast mass transport in a self-supported lithium oxygen battery cathode. *ACS Appl. Energy Mater.* **2019**, *2*, 2113–2121.
[168] Zheng, S. S.; Li, Q.; Xue, H. G.; Pang, H.; Xu, Q. A highly alkaline-stable metal oxide@metal-organic framework composite for high-performance electrochemical energy storage. *Natl. Sci. Rev.* **2020**, *7*, 305–314.
[169] Palani, R.; Karuppiah, C.; Yang, C. C.; Piraman, S. Metal-organic frameworks derived spinel $NiCo_2O_4$/graphene nanosheets composite as a Bi-functional cathode for high energy density Li-O_2 battery applications. *Int. J. Hydrogen Energy* **2021**, *46*, 14288–14300.
[170] Dou, Y. Y.; Lian, R. Q.; Zhang, Y. T.; Zhao, Y. Y.; Chen, G.; Wei, Y. J.; Peng, Z. Q. Co_9S_8@carbon porous nanocages derived from a metal-organic framework: A highly efficient bifunctional catalyst for aprotic Li-O_2 batteries. *J. Mater. Chem. A* **2018**, *6*, 8595–8603.
[171] Lv, T. T.; Zhu, G. Y.; Dong, S. Y.; Kong, Q. Q.; Peng, Y.; Jiang, S.; Zhang, G. X.; Yang, Z. L.; Yang, S. Y.; Dong, X. C. et al. Co-intercalation of dual charge carriers in metal-ion-confining layered vanadium oxide nanobelts for aqueous zinc-ion batteries. *Angew. Chem., Int. Ed.* **2023**, *62*, e202216089.
[172] Zheng, S. S.; Sun, Y.; Xue, H. G.; Braunstein, P.; Huang, W.; Pang, H. Dual-ligand and hard-soft-acid-base strategies to optimize metal-organic framework nanocrystals for stable electrochemical cycling performance. *Natl. Sci. Rev.* **2022**, *9*, nwab197.
[173] Zhen, S. Y.; Wu, H. T.; Wang, Y.; Li, N.; Chen, H. S.; Song, W. L.; Wang, Z. H.; Sun, W.; Sun, K. N. Metal-organic framework derived hollow porous CuO-$CuCo_2O_4$ dodecahedrons as a cathode catalyst for Li-O_2 batteries. *RSC Adv.* **2019**, *9*, 16288–16295.
[174] Lang, X. S.; Dong, C. X.; Cai, K. D.; Li, L.; Zhang, Q. G. Highly active cluster structure manganese-based metal organic frameworks (Mn-MOFs) like corals in the sea synthesized by facile solvothermal method as gas electrode catalyst for lithium-oxygen batteries. *Int. J. Energy Res.* **2020**, *44*, 1256–1263.
[175] Wang, J. J.; Yue, X. Y.; Liu, Z.; Xie, Z. K.; Zhao, Q.; Abudula, A.; Guan, G. Q. Trimetallic sulfides derived from tri-metal-organic frameworks as anode materials for advanced sodium ion batteries. *J. Colloid Interface Sci.* **2022**, *625*, 248–256.
[176] Zhang, W. M.; Yue, Z. W.; Wang, Q. M.; Zeng, X. X.; Fu, C. C.; Li, Q.; Li, X. T.; Fang, L. D.; Li, L. Carbon-encapsulated CoS_2 nanoparticles anchored on n-doped carbon nanofibers derived from ZIF-8/ZIF-67 as anode for sodium-ion batteries. *Chem. Eng. J.* **2020**, *380*, 122548.
[177] Xu, Z. P.; Huang, Y.; Chen, C.; Ding, L.; Zhu, Y. D.; Zhang, Z.; Guang, Z. X. MOF-derived hollow Co(Ni)Se_2/N-doped carbon composite material for preparation of sodium ion battery anode. *Ceram. Int.* **2020**, *46*, 4532–4542.
[178] Zhou, H. J.; Zhu, G. Y.; Dong, S. Y.; Liu, P.; Lu, Y. Y.; Zhou, Z.; Cao, S.; Zhang, Y. Z.; Pang, H. Ethanol-induced Ni^{2+}-intercalated cobalt organic frameworks on vanadium pentoxide for synergistically enhancing the performance of 3D-printed micro-supercapacitors. *Adv. Mater.* **2023**, *35*, 2211523.
[179] Liu, S. T.; Li, D.; Zhang, G. J.; Sun, D. D.; Zhou, J. S.; Song, H. H. Two-dimensional $NiSe_2$/N-rich carbon nanocomposites derived from Ni-hexamine frameworks for superb Na-ion storage. *ACS Appl. Mater. Interfaces* **2018**, *10*, 34193–34201.
[180] Chen, L.; Han, L. J.; Liu, X. J.; Li, Y. F.; Wei, M. D. General

synthesis of sulfonate-based metal-organic framework derived composite of M_xS_y@N/S-doped carbon for high-performance lithium/sodium ion batteries. *Chem.—Eur. J.* **2021**, *27*, 2104–2111.

[181] Atangana Etogo, C.; Huang, H. W.; Hong, H.; Liu, G. X.; Zhang, L. Metal-organic-frameworks-engaged formation of $Co_{0.85}Se$@C nanoboxes embedded in carbon nanofibers film for enhanced potassium-ion storage. *Energy Stor. Mater.* **2020**, *24*, 167–176.

[182] Ma, G. Y.; Li, C. J.; Liu, F.; Majeed, M. K.; Feng, Z. Y.; Cui, Y. H.; Yang, J.; Qian, Y. T. Metal-organic framework-derived $Co_{0.85}Se$ nanoparticles in N-doped carbon as a high-rate and long-lifespan anode material for potassium ion batteries. *Mater. Today Energy* **2018**, *10*, 241–248.

[183] Jiang, Q. Q.; Wang, L.; Zhao, W. F.; Xu, X. Y.; Li, Z.; Li, Y. X.; Zhou, T. F.; Hu, J. C. Carbon dots decorated on the ultrafine metal sulfide nanoparticles implanted hollow layered double hydroxides nanocages as new-type anodes for potassium-ion batteries. *Chem. Eng. J.* **2022**, *433*, 133539.

[184] Xie, J. P.; Zhu, Y. Q.; Zhuang, N.; Lei, H.; Zhu, W. L.; Fu, Y.; Javed, M. S.; Li, J. L.; Mai, W. J. Rational design of metal organic framework-derived FeS_2 hollow nanocages@reduced graphene oxide for K-ion storage. *Nanoscale* **2018**, *10*, 17092–17098.

[185] Deng, Q. J.; Feng, S. S.; Hui, P.; Chen, H. T.; Tian, C. C.; Yang, R.; Xu, Y. H. Exploration of low-cost microporous Fe(Ⅲ)-based organic framework as anode material for potassium-ion batteries. *J. Alloys Compd.* **2020**, *830*, 154714.

[186] Liu, L. L.; Meng, X. H.; Hu, L.; Liang, S.; Yu, L.; Liang, D. W.; Wang, L. L.; Zhou, N. N.; Yang, L.; Yang, X. L. Regular mesoporous structural FeSe@C composite with enhanced reversibility for fast and stable potassium storage. *J. Phys. Chem. C* **2021**, *125*, 15812–15820.

[187] Xie, Y. D.; Zhang, H. W.; Wu, K. D.; Wang, X. Q.; Xiong, D. P.; He, M. Fe_3C encapsulated in N-doped carbon as potassium ion battery anode with high capacity and long-term cycling performance. *J. Alloys Compd.* **2022**, *910*, 164845.

[188] Lu, X. L.; Zhang, D. D.; Zhong, J.; Wang, L.; Jiang, L.; Liu, Q.; Shao, G.; Fu, D. F.; Teng, J.; Yang, W. Y. MOF-5 as anodes for high-temperature potassium-ion batteries with ultrahigh stability. *Chem. Eng. J.* **2022**, *432*, 134416.

[189] Mahmood, A.; Ali, Z.; Tabassum, H.; Akram, A.; Aftab, W.; Ali, R.; Khan, M. W.; Loomba, S.; Alluqmani, A.; Adil Riaz, M. et al. Carbon fibers embedded with iron selenide (Fe_3Se_4) as anode for high-performance sodium and potassium ion batteries. *Front. Chem.* **2020**, *8*, 408.

[190] Nazir, A.; Le, H. T. T.; Nguyen, A. G.; Kim, J.; Park, C. J. Conductive metal organic framework mediated Sb nanoparticles as high-capacity anodes for rechargeable potassium-ion batteries. *Chem. Eng. J.* **2022**, *450*, 138408.

[191] Li, C.; Wang, K. B.; Li, J. Z.; Zhang, Q. C. Nanostructured potassium-organic framework as an effective anode for potassium-ion batteries with a long cycle life. *Nanoscale* **2020**, *12*, 7870–7874.

[192] Deng, Q. J.; Luo, Z. B.; Liu, H. X.; Wang, Y. M.; Zhou, Y. Y.; Yang, R. Self-formed carbon layer on calcium metal-organic framework and RGO composite with high-stable K-storage performance in K-ion batteries. *Appl. Surf. Sci.* **2022**, *571*, 151387.

[193] Li, A.; Li, C. F.; Xiong, P. X.; Zhang, J. F.; Geng, D. L.; Xu, Y. H. Rapid synthesis of layered K_xMnO_2 cathodes from metal-organic frameworks for potassium-ion batteries. *Chem. Sci.* **2022**, *13*, 7575–7580.

[194] Deng, Q. J.; Luo, Z. B.; Liu, H. X.; Zhou, Y. Y.; Zhou, C.; Yang, R.; Wang, L. L.; Yan, Y. L.; Xu, Y. H. Facile synthesis of Fe-based metal-organic framework and graphene composite as an anode material for K-ion batteries. *Ionics* **2020**, *26*, 5565–5573.

[195] Wang, L.; Wang, H. L.; Cheng, M. R.; Hong, Y. R.; Li, M. J.; Su, H.; Sun, J.; Wang, J. W.; Xu, Y. H. Metal-organic framework@polyacrylonitrile-derived potassiophilic nanoporous carbon nanofiber paper enables stable potassium metal anodes. *ACS Appl. Energy Mater.* **2021**, *4*, 6245–6252.

[196] Yang, H. J.; Chang, Z.; Qiao, Y.; Deng, H.; Mu, X. W.; He, P.; Zhou, H. S. Constructing a super-saturated electrolyte front surface for stable rechargeable aqueous zinc batteries. *Angew. Chem., Int. Ed.* **2020**, *59*, 9377–9381.

[197] Gou, L.; Mou, K. L.; Fan, X. Y.; Zhao, M. J.; Wang, Y.; Xue, D.; Li, D. L. Mn_2O_3/Al_2O_3 cathode material derived from a metal-organic framework with enhanced cycling performance for aqueous zinc-ion batteries. *Dalton Trans.* **2020**, *49*, 711–718.

[198] Maeboonruan, N.; Lohitkarn, J.; Poochai, C.; Lomas, T.; Wisitsoraat, A.; Kheawhom, S.; Siwamogsatham, S.; Tuantranont, A.; Sriprachuabwong, C. Dendrite suppression with zirconium(IV) based metal-organic frameworks modified glass microfiber separator for ultralong-life rechargeable zinc-ion batteries. *J. Sci.: Adv. Mater. Dev.* **2022**, *7*, 100467.

[199] Chen, T.; Wang, F. F.; Cao, S.; Bai, Y.; Zheng, S. S.; Li, W. T.; Zhang, S. T.; Hu, S. X.; Pang, H. *In situ* synthesis of MOF-74 family for high areal energy density of aqueous nickel-zinc batteries. *Adv. Mater.* **2022**, *34*, 2201779.

[200] Wang, F. F.; Lu, H.; Li, H. T.; Li, J.; Wang, L.; Han, D. L.; Gao, J. C.; Geng, C. N.; Cui, C. J.; Zhang, Z. C. et al. Demonstrating U-shaped zinc deposition with 2D metal-organic framework nanoarrays for dendrite-free zinc batteries. *Energy Stor. Mater.* **2022**, *50*, 641–647.

[201] Deng, S. Z.; Yuan, Z. S.; Tie, Z.; Wang, C. D.; Song, L.; Niu, Z. Q. Electrochemically induced metal-organic-framework-derived amorphous V_2O_5 for superior rate aqueous zinc-ion batteries. *Angew. Chem., Int. Ed.* **2020**, *59*, 22002–22006.

[202] Xiong, P. X.; Zhao, X. X.; Xu, Y. H. Nitrogen-doped carbon nanotubes derived from metal-organic frameworks for potassium-ion battery anodes. *ChemSusChem* **2018**, *11*, 202–208.

[203] He, B.; Zhang, Q. C.; Man, P.; Zhou, Z. Y.; Li, C. W.; Li, Q. L.; Xie, L. Y.; Wang, X. N.; Pang, H.; Yao, Y. G. Self-sacrificed synthesis of conductive vanadium-based metal-organic framework nanowire-bundle arrays as binder-free cathodes for high-rate and high-energy-density wearable Zn-ion batteries. *Nano Energy* **2019**, *64*, 103935.

[204] Yang, X. Y.; Sha, J. Q.; Li, W. J.; Tan, Z. L.; Hou, L. R.; Jiang, J. Z. Ternary cross-vanadium tetra-capped POMOFs@PPy/RGO nanocomposites with hybrid battery-supercapacitor behavior for enhancing lithium battery storage. *ACS Sustain. Chem. Eng.* **2020**, *8*, 4667–4675.

[205] Li, W. T.; Guo, X. T.; Geng, P. B.; Du, M.; Jing, Q. L.; Chen, X. D.; Zhang, G. X.; Li, H. P.; Xu, Q.; Braunstein, P. et al. Rational design and general synthesis of multimetallic metal-organic framework nano-octahedra for enhanced Li-S battery. *Adv. Mater.* **2021**, *33*, 2105163.

[206] Yin, C. J.; Pan, C. L.; Liao, X. B.; Pan, Y. S.; Yuan, L. Coordinately unsaturated manganese-based metal-organic frameworks as a high-performance cathode for aqueous zinc-ion batteries. *ACS Appl. Mater. Interfaces* **2021**, *13*, 35837–35847.

[207] Li, H. H.; Ma, Y.; Zhang, H.; Diemant, T.; Behm, R. J.; Varzi, A.; Passerini, S. Metal-organic framework derived Fe_7S_8 nanoparticles embedded in heteroatom-doped carbon with lithium and sodium storage capability. *Small Methods* **2020**, *4*, 2000637.

[208] Li, S. Y.; Luo, W. B.; He, Q.; Lu, J.; Du, J.; Tao, Y. H.; Cheng, Y.; Wang, H. S. A lignin-based carbon anode with long-cycle stability for Li-ion batteries. *Int. J. Mol. Sci.* **2023**, *24*, 284.

[209] Wan, J.; Li, J. F.; Xiao, Z. H.; Tang, D. D.; Wang, B.; Xiao, Y. J.; Xu, W. L. Transition bimetal based MOF nanosheets for robust aqueous Zn battery. *Front. Mater.* **2020**, *7*, 194.

[210] Wang, K. N.; Qin, M. R.; Wang, C. T.; Yan, T.; Zhen, Y. Z.; Sun, X. L.; Wang, J. W.; Fu, F. CeO_2/MnO_x@C hollow cathode derived from self-assembly of Ce-Mn-MOFs for high-performance aqueous zinc-ion batteries. *J. Colloid Interface Sci.* **2023**, *629*, 733–743.

[211] Pu, X. C.; Jiang, B. Z.; Wang, X. L.; Liu, W. B.; Dong, L. B.; Kang, F. Y.; Xu, C. J. High-performance aqueous zinc-ion batteries realized by MOF materials. *Nano-Micro Lett.* **2020**, *12*, 152.

[212] Wu, X. T.; Yin, C. S.; Zhang, M. F.; Xie, Y. Q.; Hu, J. J.; Long, R. L.; Wu, X. M.; Wu, X. W. The intercalation cathode of MOFs-driven vanadium-based composite embedded in N-doped carbon for aqueous zinc ion batteries. *Chem. Eng. J.* **2023**, *452*, 139573.

[213] Geng, P. B.; Wang, L.; Du, M.; Bai, Y.; Li, W. T.; Liu, Y. F.; Chen, S. Q.; Braunstein, P.; Xu, Q.; Pang, H. MIL-96-Al for Li-S batteries: Shape or size. *Adv. Mater.* **2022**, *34*, 2107836.

[214] Lv, T. T.; Luo, X.; Yuan, G. Q.; Yang, S. Y.; Pang, H. Layered VO_2@N-doped carbon composites for high-performance rechargeable aqueous zinc-ion batteries. *Chem. Eng. J.* **2022**, *428*, 131211.

[215] Lv, T. T.; Zhang, G. X.; Zheng, S. S.; Guo, X. T.; Chen, T. T.; Yang, S. Y.; Pang, H. *In-situ* growth of MnO_2 nanoflakes on $Co_3V_2O_8$ generating a hollow hexahedron: Zn-storage properties, and investigation of electrochemical mechanism. *Chem. Eng. J.* **2022**, *440*, 135931.

[216] Guan, C.; Sumboja, A.; Zang, W. J.; Qian, Y. H.; Zhang, H.; Liu, X. M.; Liu, Z. L.; Zhao, D.; Pennycook, S. J.; Wang, J. Decorating Co/CoN_x nanoparticles in nitrogen-doped carbon nanoarrays for flexible and rechargeable zinc-air batteries. *Energy Stor. Mater.* **2019**, *16*, 243–250.

[217] Ren, D. Z.; Ying, J.; Xiao, M. L.; Deng, Y. P.; Ou, J. H.; Zhu, J. B.; Liu, G. H.; Pei, Y.; Li, S.; Jauhar, A. M. et al. Hierarchically porous multimetal-based carbon nanorod hybrid as an efficient oxygen catalyst for rechargeable zinc-air batteries. *Adv. Funct. Mater.* **2020**, *30*, 1908167.

[218] Hou, C. C.; Zou, L. L.; Wang, Y.; Xu, Q. MOF-mediated fabrication of a porous 3D superstructure of carbon nanosheets decorated with ultrafine cobalt phosphide nanoparticles for efficient electrocatalysis and zinc-air batteries. *Angew. Chem., Int. Ed.* **2020**, *59*, 21360–21366.

[219] Bhardwaj, U.; Janjani, P.; Sharma, R.; Kushwaha, H. S. Investigation of single-metal Fe-based metal-organic framework as an electrocatalyst for a rechargeable zinc-air battery. *J. Electron. Mater.* **2023**, *52*, 917–924.

[220] Li, T. Z.; Chen, Y. H.; Tang, Z. H.; Liu, Z.; Wang, C. H. Palladium nanoparticles supported by metal-organic frameworks derived $FeNi_3C_x$ nanorods as efficient oxygen reversible catalysts for rechargeable Zn-air batteries. *Electrochim. Acta* **2019**, *307*, 403–413.

[221] Zhong, Y. T.; Pan, Z. H.; Wang, X. S.; Yang, J.; Qiu, Y. C.; Xu, S. Y.; Lu, Y. T.; Huang, Q. M.; Li, W. S. Hierarchical Co_3O_4 nano-micro arrays featuring superior activity as cathode in a flexible and rechargeable zinc-air battery. *Adv. Sci.* **2019**, *6*, 1802243.

[222] Li, J. T.; Meng, Z.; Brett, D. J. L.; Shearing, P. R.; Skipper, N. T.; Parkin, I. P.; Gadipelli, S. High-performance zinc-air batteries with scalable metal-organic frameworks and platinum carbon black bifunctional catalysts. *ACS Appl. Mater. Interfaces* **2020**, *12*, 42696–42703.

[223] Zhang, K. X.; Zhang, Y. L.; Zhang, Q. H.; Liang, Z. B.; Gu, L.; Guo, W. H.; Zhu, B. J.; Guo, S. J.; Zou, R. Q. Metal-organic framework-derived Fe/Cu-substituted Co nanoparticles embedded in CNTs-grafted carbon polyhedron for Zn-air batteries. *Carbon Energy* **2020**, *2*, 283–293.

[224] Lv, T. T.; Liu, Y. Y.; Wang, H.; Yang, S. Y.; Liu, C. S.; Pang, H. Crystal water enlarging the interlayer spacing of ultrathin $V_2O_5{\cdot}4VO_2{\cdot}2.72H_2O$ Nanobelts for high-performance aqueous zinc-ion battery. *Chem. Eng. J.* **2021**, *411*, 128533.

[225] Pourfarzad, H.; Shabani-Nooshabadi, M.; Ganjali, M. R. Novel Bi-functional electrocatalysts based on the electrochemical synthesized bimetallicmetal organic frameworks: Towards high energy advanced reversible zinc-air batteries. *J. Power Sources* **2020**, *451*, 227768.

[226] Fan, F.; Zhou, H. R.; Yan, R.; Yang, C. D.; Zhu, H.; Gao, Y.; Ma, L.; Cao, S. J.; Cheng, C.; Wang, Y. H. Anchoring Fe-N-C sites on hierarchically porous carbon sphere and CNT interpenetrated nanostructures as efficient cathodes for zinc-air batteries. *ACS Appl. Mater. Interfaces* **2021**, *13*, 41609–41618.

[227] Wang, C. H.; Kim, J. T.; Wang, C. S.; Sun, X. L. Progress and prospects of inorganic solid-state electrolyte-based all-solid-state pouch cells. *Adv. Mater.* **2023**, *35*, 2209074.

[228] Li, W. X.; Wu, C.; Ren, H.; Fang, W.; Zhao, L.; Dinh, K. N. Hybrid cobalt and iron based metal organic framework composites as efficient bifunctional electrocatalysts towards long-lasting flexible zinc-air batteries. *Batter. Supercaps* **2020**, *3*, 1321–1328.

[229] Yan, Q.; Sun, R. M.; Wang, L. P.; Feng, J. J.; Zhang, L.; Wang, A. J. Cobalt nanoparticles/nitrogen, sulfur-codoped ultrathin carbon nanotubes derived from metal organic frameworks as high-efficiency electrocatalyst for robust rechargeable zinc-air battery. *J. Colloid Interface Sci.* **2021**, *603*, 559–571.

[230] Zhang, G. X.; Jin, L.; Zhang, R. X.; Bai, Y.; Zhu, R. M.; Pang, H. Recent advances in the development of electronically and ionically conductive metal-organic frameworks. *Coord. Chem. Rev.* **2021**, *439*, 213915.

[231] Hossain, M. A.; Tulaphol, S.; Thapa, A. K.; Rahaman, M. S.; Jasinski, J. B.; Wang, H.; Sunkara, M. K.; Syzdek, J.; Ozdemir, O. K.; Ornstein, J. M. et al. Metal-organic framework separator as a polyselenide filter for high-performance lithium-selenium batteries. *ACS Appl. Energy Mater.* **2021**, *4*, 13450–13460.

[232] Yang, H. J.; Qiao, Y.; Chang, Z.; Deng, H.; He, P.; Zhou, H. S. A metal-organic framework as a multifunctional ionic sieve membrane for long-life aqueous zinc-iodide batteries. *Adv. Mater.* **2020**, *32*, 2004240.

[233] Li, C. W.; Zhang, Q. C.; Li, T. T.; He, B.; Man, P.; Zhu, Z. Z.; Zhou, Z. Y.; Wei, L.; Zhang, K.; Hong, G. et al. Nickel metal-organic framework nanosheets as novel binder-free cathode for advanced fibrous aqueous rechargeable Ni-Zn battery. *J. Mater. Chem. A* **2020**, *8*, 3262–3269.

[234] Li, R. R.; Ke, H. Z.; Shi, C.; Long, Z. W.; Dai, Z. X.; Qiao, H.; Wang, K. L. Mesoporous RGO/$NiCo_2O_4$@carbon composite nanofibers derived from metal-organic framework compounds for lithium storage. *Chem. Eng. J.* **2021**, *415*, 128874.

[235] Li, C. F.; Li, A.; Li, M. J.; Xiong, P. X.; Liu, Y. S.; Cheng, M. R.; Geng, D. L.; Xu, Y. H. Ultrafast synthesis of layered transition-metal oxide cathodes from metal-organic frameworks for high-capacity sodium-ion batteries. *ACS Appl. Mater. Interfaces* **2022**, *14*, 24462–24468.

[236] Zhang, X. J.; Gao, X. Y.; Hong, K.; Jiang, J. L.; Zhang, L. J.; Chen, J.; Rao, Z. H. Hierarchically porous carbon materials derived from MIL-88(Fe) for superior high-rate and long cycling-life sodium ions batteries. *J. Electroanal. Chem.* **2019**, *852*, 113525.

[237] Tan, X. H.; Liu, J. W.; Huang, Q. H.; Wu, Y. J.; Lin, X. M.; Zeb, A.; Yuan, Z. Z.; Xu, X.; Luo, Y. F. Efficient vapor-solid fluorination synthesis of MOF-derived MnF_2/C for superior lithium storage with boosted kinetics. *J. Alloys Compd.* **2022**, *895*, 162569.

[238] Kon, K.; Uchida, K.; Fuku, K.; Yamanaka, S.; Wu, B.; Yamazui, D.; Iguchi, H.; Kobayashi, H.; Gambe, Y.; Honma, I. et al. Electron-conductive metal-organic framework, Fe(dhbq) (dhbq = 2,5-dihydroxy-1,4-benzoquinone): Coexistence of microporosity and solid-state redox activity. *ACS Appl. Mater. Interfaces* **2021**, *13*, 38188–38193.

[239] Na, Z.; Yao, R. F.; Yan, Q.; Wang, X. R.; Sun, X. D. Metal-organic frameworks derived in-based nanoparticles encapsulated by carbonaceous matrix for highly efficient energy storage. *Appl. Surf. Sci.* **2020**, *513*, 145894.